

## Retrospect and Prospect of the SR Center

**Toshiaki Ohta**

*Research Organization of Science & Engineering, Ritsumeikan University, 1-1-1 Noji-Higashi, Kusatsu 525-8577, Japan*

### **Abstract**

The compact storage ring, AURORA was installed in Ritsumeikan University in 1995 and started its operation in the next year. The SR center was established in the same year. Since then, the ring has been operated without any serious trouble until 2021, when a water leak trouble happened in the RF cavity in the ring. It took 9 months to restart operation. As a result of it, we could not use SR almost one year. This was the first serious trouble, but it might be a good opportunity to look back upon the past activities of the SR center and to think over the future plans. I have been the director of the center for twelve years from fiscal 2006 to fiscal 2018. As a living witness of the center, it might be worthwhile to review the history of the SR center.

The history of the center can be roughly divided to two phases: the first is from 1996 to 2006 and the second from 2006 to the present. In the first phase, the most brilliant scientific output was the fabrication of micro-devices using the LIGA technique, while in the second phase, scientific activities have been focused on characterization of functional materials, especially secondary batteries by using synchrotron radiation-based spectroscopies. In this review article, I will describe the development of beamlines and selected activities in each phase from my own personal judgement and also address the future plans of the center.

## 1. Phase I

### 1.1 Development of a compact ring, AURORA

Synchrotron radiation (SR) is known to be a kind of very intensive X-ray sources with several unique features, produced from electron accelerators, such as synchrotron and storage ring. In 1960s, parasitic uses of storage rings for high energy physics demonstrated the high potential of synchrotron radiation as a light source in vacuum ultraviolet (VUV) and X-rays. In 1970s, several storage rings have been constructed just for use of SR, first small rings for VUV and later large rings for X-rays. In Japan, a small VUV ring, “INSSOR” was constructed at Institute of Nuclear Physics in Tanashi in 1975 and the Photon Factory (PF) project started in 1978 to construct 2.5 GeV storage ring for providing intense light extending to X-rays in KEK, Tsukuba. This was a big national project, whose budget was almost 30 BY. In 1982, PF has produced very intense X-rays and gave big impact not only to academia but also to industries. SR is of course very promising light source for characterizing materials, but also for X-ray lithography to produce very fine semiconductors. Thus, another target was to construct a compact and less expensive SR accelerator. Some groups pursued to construct a table-top SR accelerator for X-ray lithography and a few groups in the world succeeded to construct compact rings. In Japan, Sumitomo Heavy Industries Ltd. (SHI) challenged this project and successfully constructed the world’s smallest storage ring, named AURORA in 1989 [1]. This is composed of one body superconducting magnet, in which high energy electrons runs in a circular orbit, as shown in Fig. 1. The diameter of the electron orbit was just one meter. The key factor was how to inject electrons in such a circular one body ring. Sumitomo group found a unique injection method [2]. They made use of a resonance of electron orbit at 150 MeV, where electrons injected can be stored in the ring with high efficiency. By use of a compact racetrack microtron, electrons accelerated to 150 MeV are injected in the ring and subsequently, further accelerated up to 575 MeV, which is limited by the available magnetic field. This electron energy is smaller than other light sources, such as UVSOR. However, thanks to the use of a superconducting magnet, the SR emitted from the ring extends to high photon energies, whose critical wavelength is 1.5 nm. The horizontal and vertical beam sizes ( $\sigma_x$ , and  $\sigma_y$ ) are 1.2 and 0.14

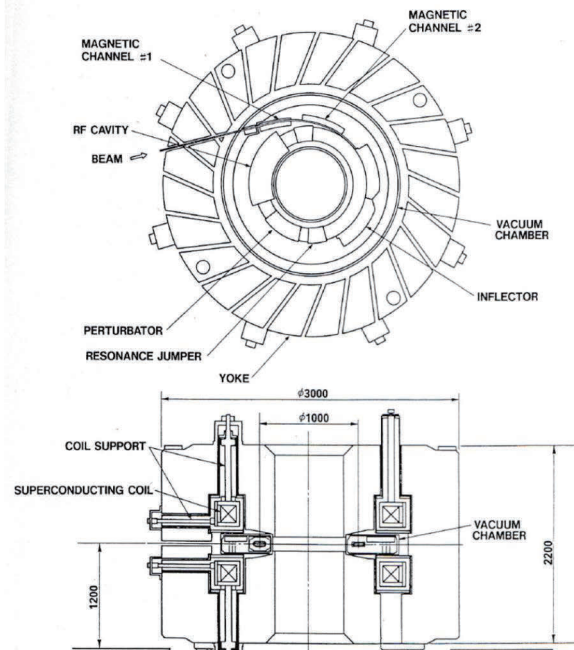


Fig. 1. The storage ring, AURORA developed by SHI. (a) plan view and (b) sectional view.

mm, respectively and the emittance is about 100 times larger than that of the PF ring, which is not suitable for spectroscopic applications, but is an ideal light source for X-ray lithography. The first machine, AURORA was successfully constructed and several demonstrative experiments were performed. However, no customer appeared at all, even though the machine itself was very compact and effective. It might be because the enthusiasm for the SR as the light source for X-ray lithography has almost cooled down in 1990s.

## 1.2 Introduction of the AURORA in BKC of Ritsumeikan University

Ritsumeikan University is the biggest private university in Kansai area, established in 1900. Originally, it was located in Kinugasa, Kyoto. With increase of students, the university decided to open a new campus in Kusatsu area in Shiga prefecture in 1995. The new campus is called, Biwako-Kusatsu campus (BKC), where the faculty of science and engineering moved from Kinugasa campus. In occasion of the movement, the head of the university planned to introduce an edge-cutting facility as a symbol of the new campus. SR facility was the best candidate. In early 1990s, Photon Factory in KEK, UVSOR in Institute of Molecular Science and TERAS in Electron Technical Laboratory were the facilities operating and SPring-8 started construction in 1992. The committee organized in the university in 1992, headed by the chief director Mr. Kawamoto, finally chose the AURORA developed by SHI. Total cost was about 3 BY, quite expensive for the facility installed in a private university. Note that all the cost was paid by the donation of the alumni association of Ritsumeikan University. It must be a big challenge and also a big gambling. The AURORA ring and an electron injector, race track microtron, were installed in 1995 and the first SR beam was observed in the next year [3]. Figure 2 is a photo of the committee members and staffs involved with the AURORA storage ring just installed in 1995.



**Fig.2.** Photo of the AURORA storage ring installed in the SR center with staffs and committee members involved in the introduction of the ring, taken in December, 1995.

### 1.3 Management of the SR center

The SR center was established in 1995 and the first director of the SR center was assigned to Prof. Hiroshi Iwasaki (Fig. 3), who used to be the director of the Photon Factory for 1991-1994 and moved to Ritsumeikan University as a professor of Science and Engineering in 1994 after retirement of KEK. He specialized in X-ray diffraction and scattering, using synchrotron radiation. The second director from 1997 to 1999 was Dr. Shigero Ikeda, emeritus professor of Osaka University. He specialized in analytical chemistry and made efforts to reinforce beamlines especially for spectroscopies. Third director was succeeded again by Prof. Iwasaki for 2000 to 2003.



**Fig. 3** Prof. Hiroshi Iwasaki, the first director of the SR center.

The head of the university first thought about the SR center as a gold mine of the university and the liaison office deeply involved in the management and invited industries in Kasai area to use the center. The head's goal was to make the center financially independent from the university by making up for the running cost of the center by the incomes from users and funds of the government. In 1996, the liaison office organized the consortium for industrial applications of synchrotron radiation, named "SRAC" (Synchrotron Radiation Applications Consortium) (放射光産業利用技術懇談会) to encourage user activities of the SR center, especially from industries. At that time, synchrotron radiation facilities in Japan, such as Photon Factory and UVSOR were mostly for academia. The SR center was the first facility encouraging industrial applications. More than 20 industries in Kansai area, headed by Kansai Electric Power Co. Inc., joined this community. The community organized seminars for topics of synchrotron radiation, tours to the SR center, training courses with technical advises for the community members.

For several years, the center and the liaison office had struggled to increase the income and applied every possible fund of the government, but in vain. The situation changed in 2002, when the MEXT started the nanotechnology supporting program, which encouraged activities for nanotechnologies and specified 'synchrotron radiation' as one of the advanced tools. Fortunately, the SR center was chosen as a synchrotron radiation group member with SPring-8 to support the experiments related to nanotechnologies. This program had worked from 2002 to 2007, subsidizing the budget for beamline improvement, as well as covering user's fee. Especially, it was greatly helpful that the program covered the labor costs of 3~4 supporting staffs.

The fourth director (2004-2005) was Prof. Atsuhiko Okamoto, moved from Toyota Central Laboratory. He specialized in XAFS spectroscopy, putting forth his best efforts in nanotechnology user service.

### 1.4 Development of the beamlines

In the ring, there are 16 ports available for beamlines. In the first 2 years, 10 ports were occupied by beamlines, which were either newly constructed or transferred from other facilities. The whole view of the SR center in 1996 is shown in Fig. 4 and Table 1 lists the beamlines installed in Phase I from 1996 to 2006.

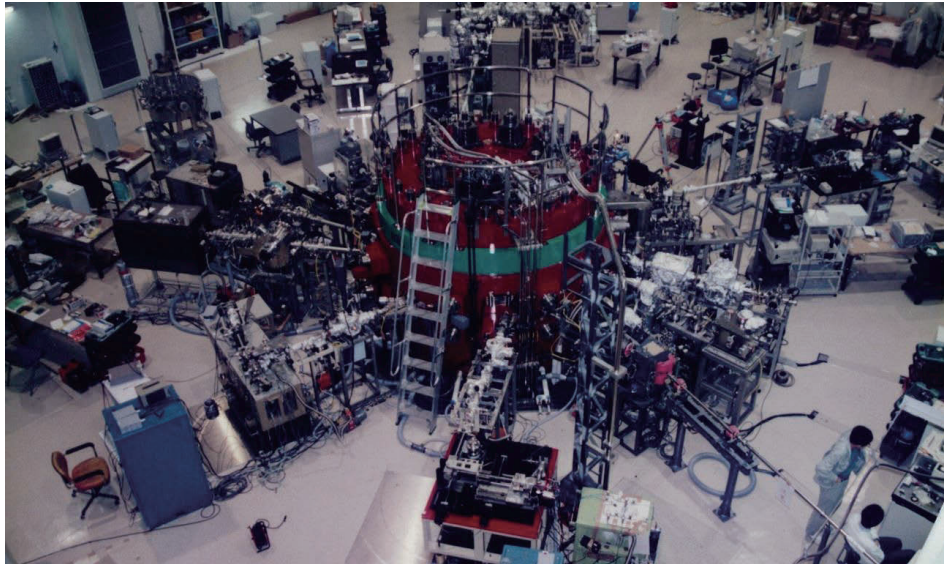
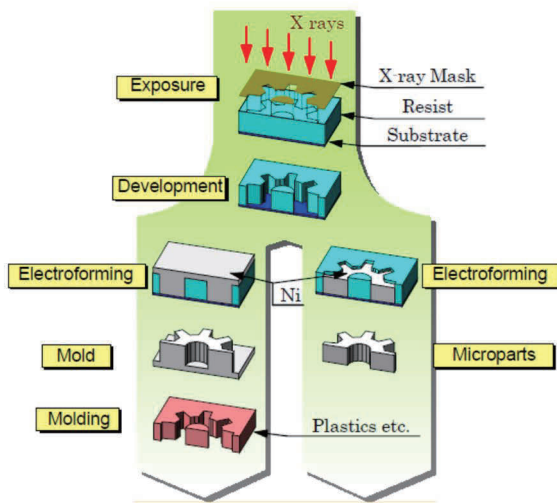


Fig. 4 Photo of the SR center in 1996. 9 beamlines had been installed.

Table 1. List of the beamlines in Phase I from 1996 to 2006

Beamline	Year: Method (Available energy range/eV)
BL-1	1996: Soft X ray spectroscopy (500-4000) →2000: X-ray Diffraction and scattering (4000-8000) --→
BL-2	1996: VUV spectroscopy (5-600) -----→
BL-3	1997: X-ray diffraction (4000-8000) →2000: X-ray Reflectivity (2000-10000) ----→
BL-4	1997: XAFS (3400- 9000) -----→
BL-5	→2000: Multi LIGA -----→
BL-6	1996: LIGA process (2000-10000) -----→
BL-7	→2002: 2D-PES (35-130 ) -----→
BL-8	1997: PES with Ion scattering (5-700) -----→
BL-10	1997: Soft X-ray XAFS (1000-4000) -----→
BL-12	1997: Soft X-ray microcopy (280-540) -----→
BL-13	1997: X-ray fluorescence analysis (3000-10000) →2002: LIGA process -----→
BL-14	1997: SR stimulated processing (50-2000) -----→
BL-15	1999: X-ray diffraction → 2000: Multi-stage LIGA -----→

Among the above beamlines, four beamlines should be noted. First one is the LIGA beamline (BL-6). Although the fever for the application of SR to X-ray lithography was cooled down in 1990s, a new method has emerged instead. This was so-called “deep lithography”, or “LIGA”, which is the abbreviation of **L**ithographie, **G**alvanoformung and **A**bformung, developed by E.W. Becker and W. Ehrfeld in Karlsruhe Research Center, West Germany in early 1980’s [4,5]. Their original plan was to develop micro filter for isotope separation by using the X-ray lithography technique and it turned out to be a very promising technique to fabricate micromachines and microsensors. The LIGA process is schematically shown in Fig.5.



**Fig. 5.** Flow of the LIGA process. Right side is for positive micropart and left side for negative one.

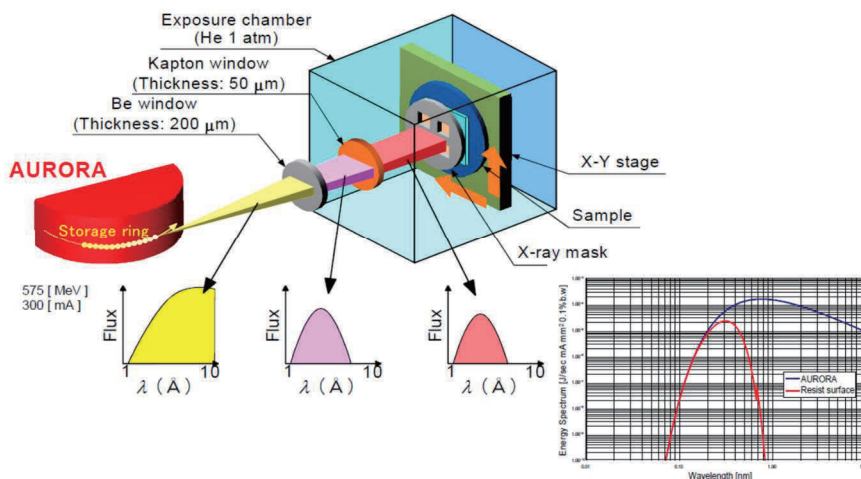


**Fig. 6.** Schematic figure of a typical LIGA beamline. SR X-rays in the longer wavelength are filtered out by using Be and Kapton window, as shown in the inset figure. Sample and X-ray mask are set on a X-Y stage. Exposure chamber is filled with 1 atm He gas. In the inset graph, the blue and red lines are the photon intensity distribution of SR from the ring and that on the resist, respectively.

Firstly, X-rays irradiate a polymer resist, PMMA (polymethyl methacrylate) through an X-ray mask with a specific pattern. Second is the development. Chemical bonds in the irradiated parts are destroyed and easily solved by organic solvent. As a result of it, remained part has a microstructure. Third is the electrodeposition. The microstructure formed in PMMA is transferred to the electrodeposited Ni plate. Right side in Fig. 4 is just for fabrication of Ni microparts and the left side is for negative structured parts. The advantage of using SR is its high intensity and high directionality. High aspect ratio, such as 100 vs. 1, can be easily obtained. Figure 6 shows a typical LIGA beamline. Profs. S. Sugiyama and O. Tabata energetically pushed the LIGA project and increased the LIGA beamlines up to 4 in a few years. A number of industries had keen interest in the LIGA experiment and took part in the collaboration with their laboratories.

Second unique beamline is BL-8, where a soft X-ray spectroscopic beamline equipped with a grazing incidence monochromator is combined with a medium energy ion scattering (MEIS) spectroscopy. The grazing incidence monochromator was newly designed and constructed, which used a varied line spacing grating [6], covering the photon energy from 5 to 700 eV with the photon flux of  $10^{10}$ - $10^{11}$  photons/s/300 mA, whose beamline layout is shown in Fig. 7 and specifications are listed in Table 2. High energy resolution PES (Special version of PHI model) was equipped at the end of the station. Typical photoelectron spectra taken in this beamline [7] are shown in Fig. 8, indicating the comparable quality with those [8] taken at MAX-2, the third generation ring.

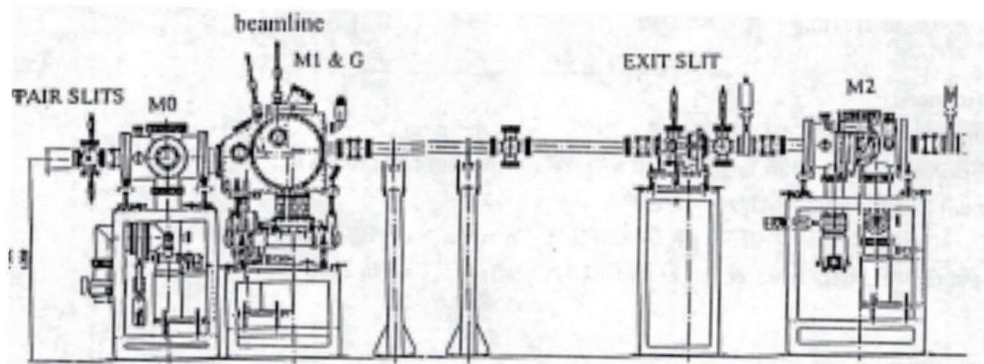


Fig. 7. Beamline layout of BL-8, equipped with a varied-line spacing grating.

**Table 2** Specifications of BL-8

---

Available Photon Energy : 5 ~ 700 eV
Energy Resolution ( $E/\Delta E$ ): 5000~1500
Photon Flux: $10^{10}$ ~ $10^{11}$ photons/s/300 mA
SR Beam Acceptance: $10.5 \text{ mrad}^H \times 3.0 \text{ mrad}^V$
Beam size on target: $2 \text{ mm}^H \times 1 \text{ mm}^V$
Grating: Varied-line-spacing plane grating (Hitachi, mechanically ruled, 400 and 1800 l/mm)
Mirrors: $M_0$ =cylindrical, Si, $M_1$ =plane, quartz, $M_2$ =toroidal, quartz

---

The MEIS system consisted of an ion accelerator (30 ~ 125 kV), a switching magnet and an ion scattering chamber, in which a high resolution toroidal electrostatic analyzer was mounted on a rotatable table. A duoplasma ion source of the hollow cathode type generated dense plasmas of  $H^+$ ,  $He^+$  and  $Ne^+$  and provided intense ion beams with high emittance. Typical ion beam currents on a target were 20 and 3 nA for 100 keV  $He^+$  and  $H^+$  ions, respectively. A sample could be transferred to the PES chamber without exposing to air. This beamline was called, “SORIS” (Synchrotron Orbital Radiation and Ion Scattering). The schematic SORIS system is shown in Fig. 9 and specifications are listed in Table 3.

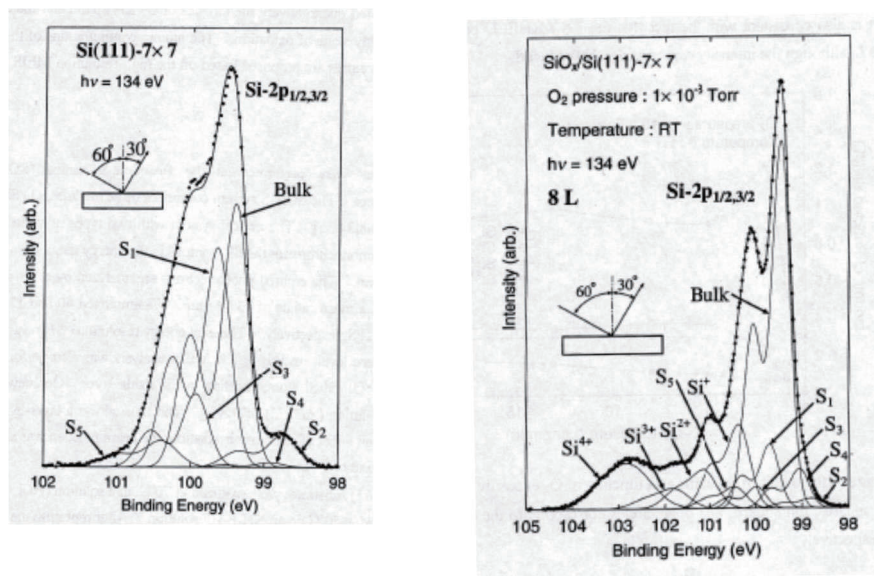


**Fig. 8.** Si 2p PES spectra of a Si(111)7x7 clean surface(left) and half oxidized Si(111)(right) [7]. Observed spectra were best-fitted by the simulated ones convoluted by several components. S<sub>1</sub>-S<sub>4</sub> are the adatoms, rest atoms, atoms bonding to the adatoms and dimers, respectively. The origin of S<sub>5</sub> is still unknown.

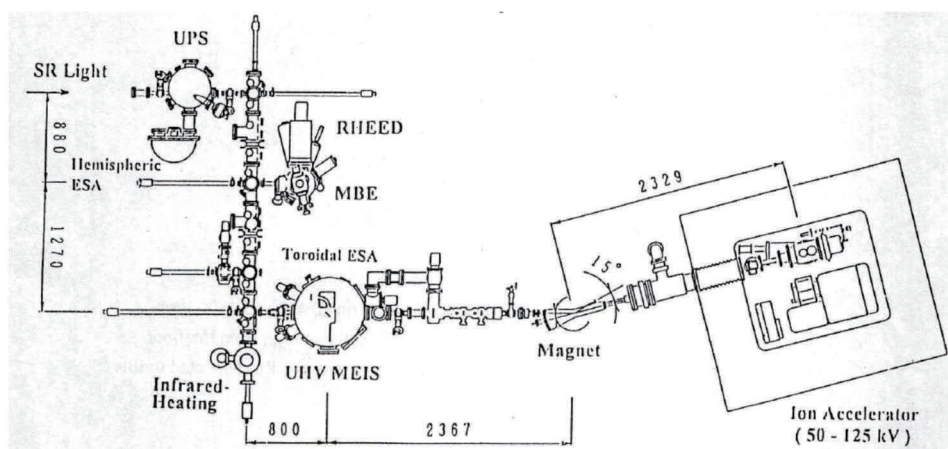


**Fig. 9.** Schematic layout of the SORIS beamline (BL-8).

**Table 3** Specifications of MEIS in the SORIS beamline

Vacuum: $2 \times 10^{-10}$ Torr (base), $8 \times 10^{-10}$ Torr (in operation)
Ion Beams: 30~125 keV He <sup>+</sup> (20 nA), H <sup>+</sup> (3 nA) and Ne <sup>+</sup> (10 nA)
Toroidal Electrostatic Analyzer: $\Delta E/E=9 \times 10^{-4}$
MBE: 3 K-Cells +RHEED (RT~850°C), Vacuum $1 \times 10^{-10}$ Torr. (base)
Sample Heating: Infrared Light under UHV from RT up to 1000°C.

The third unique beamline is BL-12, “soft X-ray microscopy”. Prof. Kihara of Kansai Medical University installed a transmission X-ray microscope in 1997, which was initially used at UVSOR. At that time, this was the fourth soft X-ray microscopy beamline in the world. This consists of a plane mirror to cut high energy parts of synchrotron, CZP (condenser zone plate), a pinhole, sample in air, OZP (objective zone plate) and a CCD camera, as shown in Fig. 10. The two zone plates are key optical elements, whose specifications are listed in Table 4.

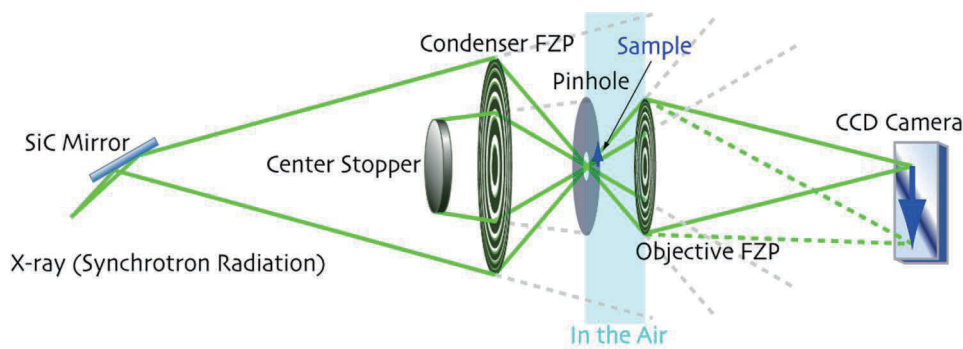


**Fig.10.** Optical layout of the soft X-ray microscopy beamline, BL-12

**Table 4.** Specifications of the zone plate

	CZP	OZP
Diameter/mm	9000	50
Number of zones	41890	277
Outermost zone width/nm	53.7	45
Zone material	Ge ( 300 nm thick)	Ni(130 nm thick)

This beamline was aimed to image objectives in the water window region, 2.2~4.3 nm, where images of those in water can be obtained. Spatial resolution is determined by the outermost zone width of the zone plates. Thanks to the high performance of the CZP [9], it was estimated to be 50 nm and was further experimentally confirmed at the photon energies of 2.4 and 3.2 nm [10].

The fourth unique one was BL-7 soft X-ray grazing incidence monochromator beamline, equipped with a modified Rowland-mount spherical grating, covering the photon energy from 35 to 130 eV. This beamline was constructed by the fund of the nanotechnology supporting program

in 2002. At the end of the station, 2-D Display-type Analyzer (DIANA), developed by Prof. Daimon of Nara Institute of Science and Technology, was installed [11], aiming at 2 D angle-resolved photoelectron spectroscopy. The electron analyzer is shown schematically in Fig. 11. Photoelectrons with same kinetic energy emitted within a solid angle of  $\pm 50^\circ$  can be detected by an MCP at the same time. This analyzer enables to obtain 2 D angular distribution of the photoelectrons. The energy and angular resolutions are 1% and  $1^\circ$ , respectively. Typical acquisition time was 5 min. By changing the incident photon energy, 3 D band structures can be obtained in a wide reciprocal space, for example,  $\pm 2.3 \text{ \AA}^{-1}$  at kinetic energy of 36 eV. Furthermore, linearly polarized SR light enables the analysis of the atomic orbital composition of each band.

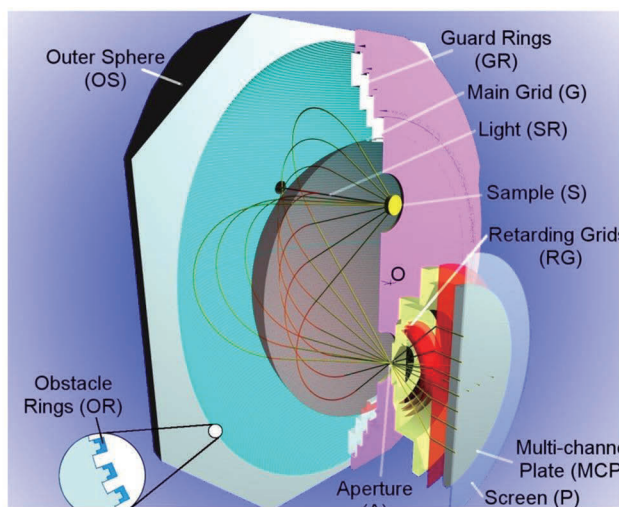


**Fig. 11.** Schematic figure of the 2-D display type analyzer (DIANA). A linearly polarized light is introduced through a hole in the obstacle ring (OR). A spherical electric field applied between the OR and a main grid (MG) makes photoelectrons with a selected kinetic energy focus at the aperture. Photoelectrons are multiplied by micro-channel plate (MCP) and projected on to a fluorescent screen keeping the emission angle.

## 1.5 Scientific outputs

### (1) Fabrication of micromachines and microstructures

As described in the beamline session, the LIGA process emerged as a promising technique to fabricate micromachines. The first important process is to prepare an X-ray mask. Prof. Sugiyama has established the method of making an X-ray mask, whose process is schematically shown in Fig. 12. In collaboration with Optonics Precision Co. Ltd. and NTT Advanced Technology Co. Ltd., he developed an Au/polyimide X-ray mask of micron precision, a Ta/SiC X-ray mask of submicron precision, respectively.

Prof. Sugiyama's group fabricated several kinds of microstructures and micromachines to demonstrate the effectiveness of the LIGA technique using synchrotron radiation, as shown in Fig. 13. In fact, they obtained the aspect ratio of as high as 100 vs. 1. With this technique, high precision microstructures made of various materials such as plastic, metal and ceramics. This was the first demonstration performed in Japan, giving a great impact to industries [12].

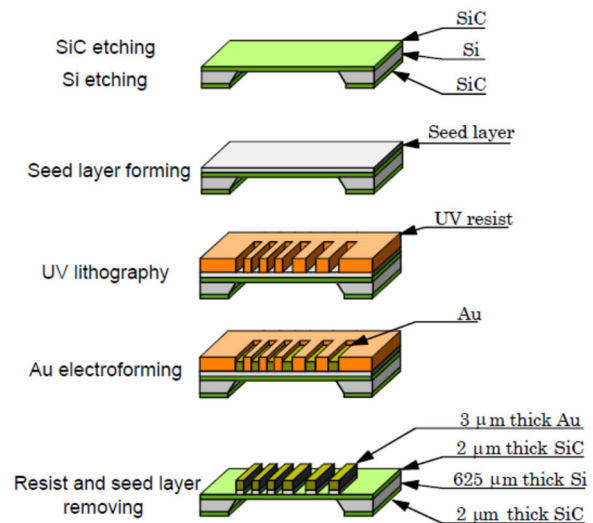


Fig. 12. Process of making an X-ray mask.

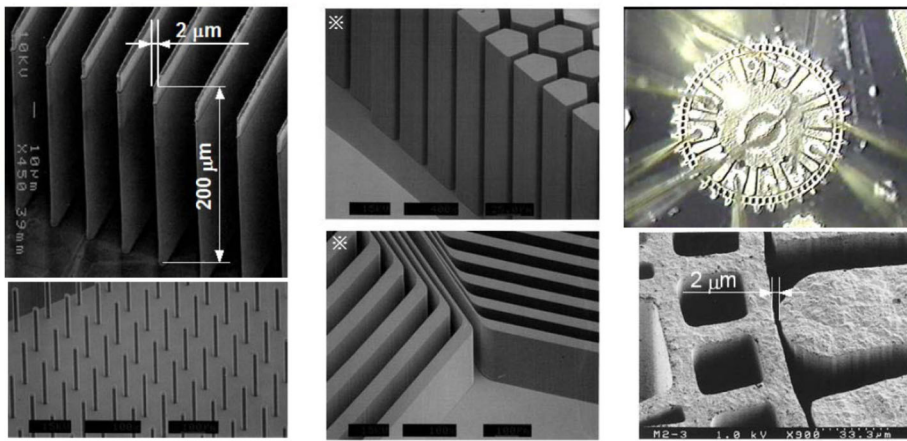


Fig. 13. Typical examples of the products by the LIGA technique in the SR center.

However, this normal deep lithography and LIGA process can only fabricate microstructures with vertical wall, which limits the applications.

One of the methods to overcome this limitation is to move either X-ray mask or a resist. The concept of the moving mask deep X-ray lithography ( $M^2DXL$ ) [13] is shown in Fig. 14.

Since the processed depth of resist depends on the absorbed energy in the surface, an X-ray mask is moved during exposure to yield a well-controlled energy distribution on the resist to define the processed depth. By combining various mask patterns and mask movement trajectory, microstructures with free shaped wall can be realized [14].

This moving mask method was further developed by Prof. Sugiyama as the PCT (Plane-pattern to Cross-section Transfer) method, as schematically shown in Fig. 15. By moving a wedge-shaped X-ray mask, triangular walls can be produced. Further, by rotating the mask by  $90^\circ$  and moving it as well, pyramidal needle arrays can be obtained. With this technique, many pieces with several kinds of microstructures were produced as shown in Fig. 16 [15]. In particular, the bottom right photo shows a model for micro needles, expecting medical applications, although not realized yet.

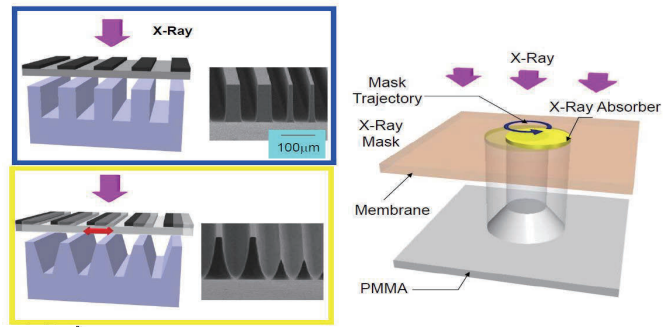


**Fig. 14.** Concept of the moving mask method. Upper left is the conventional fixed mask, while lower left is the moving mask, which makes any kind of shape according to the moving pattern. Right figure shows how to fabricate a cone-shaped microstructure.

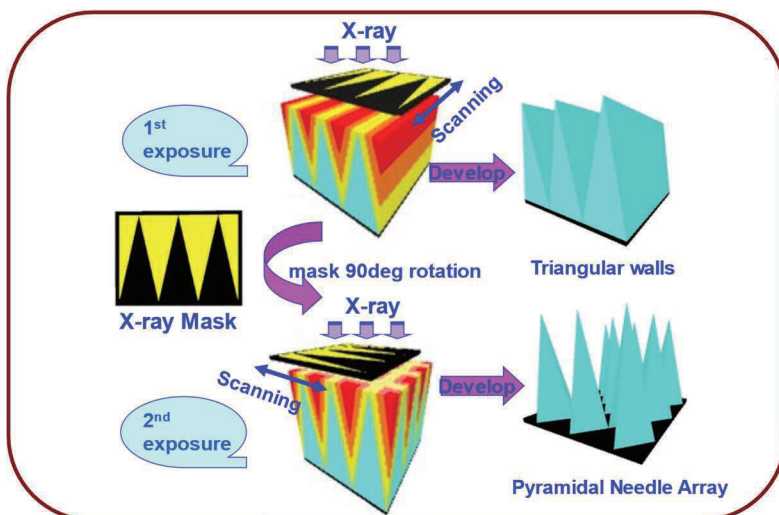


**Fig.15.** Double PCT method. The first exposure with moving mask produces triangular walls, while the second exposure with moving the mask  $90^\circ$  rotated produces a pyramidal needle array.

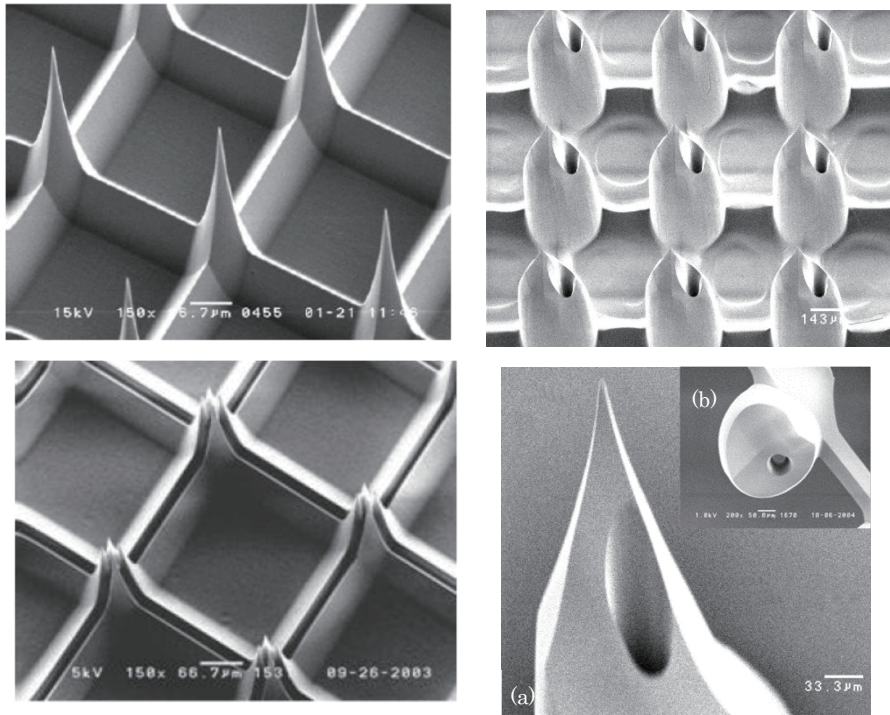


**Fig. 16.** Several kinds of products fabricated by the double PCT method.

Another development was an application to direct etching. Conventional LIGA process needs wet etching using organic solvents, but by using PTFE (polytetrafluoroethylene) as a resist, it is possible to perform dry etching. First demonstration was performed by Zhang and Kato [16], as schematically shown in Fig. 17. Later, it was found to heating PTFE up to 200 °C enhanced the etching rate dramatically, as shown in the bottom right graph in Fig. 17 [17]. This technique greatly saves the process for microfabrication, but it also needs extra apparatus to remove toxic fluorine gas. There were also several industries which produced commercial products, such as Sumitomo Heavy Co. Ltd. and STARLITE Co. Ltd. Typical example is a micro fluid passage for medical application. Figure 18 shows the process of fabricating a number of microfluids by using the injection mold technique.

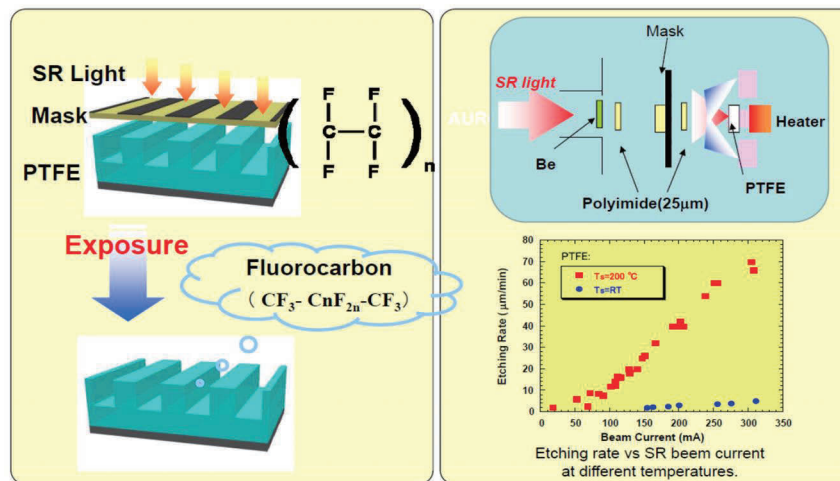


Fig. 17. The LIGA method for dry etching by using PTFE as a resist.

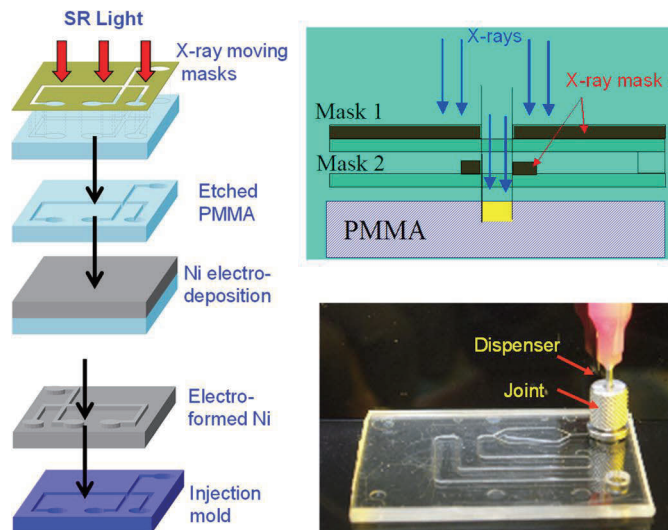


Fig. 18. The LIGA process to fabricate a micro fluid passage, developed by STARLITE Co. Ltd. By using the electroformed Ni as a template, a number of products were produced with the injection mold technique. Courtesy of Dr. Kurokawa (STARLITE Co. Ltd.)

## (2) Combined use of MEIS and PES for surface structure analysis

As described above, Prof. Kido constructed a unique beamline, where MEIS and PES experiments using synchrotron radiation can be performed for any sample without exposing to air.

With this beamline, his group actively studied surface electronic and atomic structures of several interesting materials [18-31].

The first target was SrTiO<sub>3</sub>(STO) (001) [18], which is well known as a lattice-matched substrate suitable for the epitaxial growth of high-T<sub>c</sub> cuprate films. It has been pointed out that the atomic

species and their alignments in the terminating layer of the substrate crucially influence the resulting surface reaction for the atomically controlled heteroepitaxial growth. As the SrTiO<sub>3</sub> crystal has a structure stacked alternately by two kinds of nonpolar atomic planes, i.e., SrO and TiO<sub>2</sub>, along the c-axis direction, different surface terminations with either SrO or TiO<sub>2</sub> at the (001) top layer are possible. Thanks to the high surface sensitivity of PES and MEIS, they determined the fraction of TiO<sub>2</sub> layer and O vacancy in the topmost layer quantitatively for the TiO<sub>2</sub> terminated surface as a function of annealing temperature. Results of the MEIS and UPS are shown in Figs. 19 and 20, respectively.

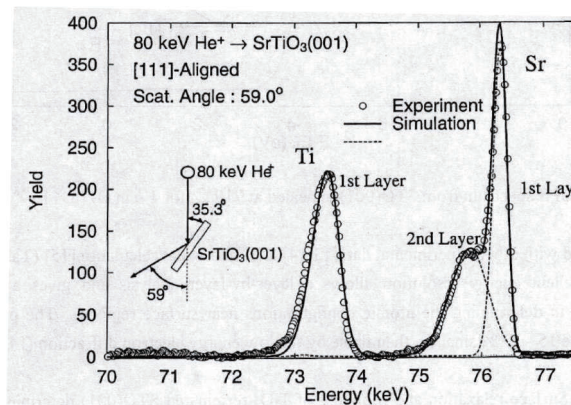


**Fig. 19.** MEIS spectrum of SrTiO<sub>3</sub>(001) annealed at 650°C for 1h in O<sub>2</sub>(5×10<sup>-6</sup> Torr).

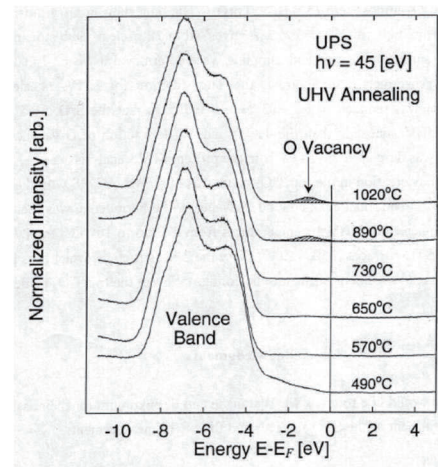


**Fig. 20.** PES spectra of SrTiO<sub>3</sub>(001) annealed in UHV at elevating temperatures for 1 h.

The MEIS spectrum in Fig. 19 shows the contributions from Sr and Ti layers. From the ratio of the scattering yield from the top layer Sr to that of Ti, it turned out that 12 % of the topmost layer was replaced to the SrO face. Figure 20 shows the valence band spectra, in which non-bonding O 2p appears at 5 eV and bonding O2p and Ti3d+4p at 7 eV. The new band appeared at 1.2 eV below the Fermi edge above 890°C was assigned to the surface O vacancy. This experiment demonstrated how effective the combined use of MEIS and PES is to clarify the topmost surface structures.

They conducted the combined experiments of PES and MEIS spectra for the initial oxidation of Si(111) [7,20], 6H-SiC(0001) surface [21,24,25,26], thin Ni layers/Si(111) [22,30], Ni/SiC(0001)[27], C-terminated 6H-SiC(0001)[28], Ni deposited SiC [31], HfO<sub>2</sub>/Al<sub>2</sub>O<sub>3</sub> on nitrized and oxidized Si substrate[29], etc. Among them, the work on Ni/Si(111) is picked up. In fact, there have been numerous reports on the initial growth process for Ni-deposited Si substrates before and after annealing from viewpoints of application to device fabrications and also of fundamental interest. Prof. Kido's group also studied the initial growth processes of Ni on Si(111)

as-grown and post-annealed by using the unique combination of MEIS and PES. Figure 21 shows MEIS spectra from Ni/Si(111) deposited at RT with several Ni coverages. By the spectral deconvolution, they discriminated the peaks from atop Si, buried Si and Ni silicide, as well as substrate Si. Figure 22 shows Si 2p spectra of the Ni/Si(111) with several coverages. They observed three components in the Si 2p spectra with binding energies of 98.8, 99.3 and 99.9 eV scaled from the Fermi level, which are assigned, respectively to (1) the 1st-layer Si atoms bonded to the Si adatoms, (2) the Si adatoms together with the 1st- (non-bonded to the Si adatoms) and 3rd-layer Si atoms and (3) the bulk NiSi<sub>2</sub> (4th and deeper layers Si atoms). By the results from MEIS and PES, they found that a thin NiSi<sub>2</sub>-like layer is initially formed at the interface. With increasing Ni-coverage the surface becomes Ni-rich silicides and finally a Ni layer stacks on the silicide layer for Ni-coverage more than 10 ML. From the annealing experiments, they found annealing at 500°C leads to formation of a NiSi<sub>2</sub> epitaxial layer, onto which a small amount (~0.2 ML) of Si adatoms are located.

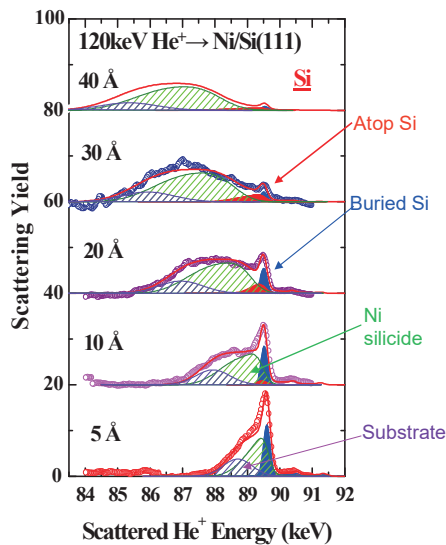


**Fig.21** MEIS spectra from Si of Ni/Si(111) deposited at RT, observed for 120 keV He<sup>+</sup> ions incident along the [001] axis and backscattered to the [110] direction for several Ni coverages on Si(111) [22]. Red curves are the best-fitted spectra assuming appropriate elemental depth profiles. Filled red and blue areas are the components from atop Si and incorporated in Ni layer, respectively. Slashed green and purple areas deconvoluted come from Ni-silicide and Si substrate, respectively.

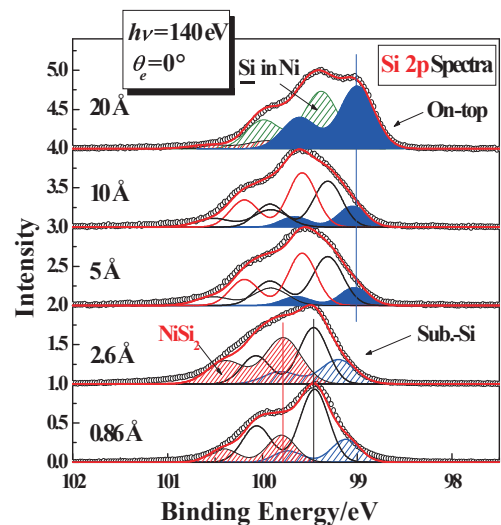


**Fig.22.** Si 2p core level spectra from Ni/Si(111) with several Ni coverages, observed at photon energy of 140 eV under normal emission[22]. Each observed spectrum was deconvoluted into components from Si on top (filled blue area), incorporated in Ni (slashed green area) and NiSi<sub>2</sub> (slashed red area). The blue, black and red bars indicate the energy positions (Si 2p<sub>3/2</sub>) for the surface-segregated Si, bulk Si and NiSi<sub>2</sub>, respectively.

### (3) Band dispersions obtained with the DIANA electron analyzer

To study band dispersions of materials is the most fundamental process to understand the electronic and magnetic properties of materials intuitively. Angle resolved photoelectron spectroscopy (ARPES) is a typical method to get information of band dispersion. However, it takes a lot of time to the band dispersion of the entire BZ by using a conventional ARPES. ‘DIANA’ installed in BL-7 is a powerful apparatus for that purpose. The entire Brillouin Zone (BZ) in the  $k_x, k_y$  plane can be extracted by stacking a series of PEAD (Photoelectron angular distribution) patterns with different binding energies and picking up spectra  $E_B(k_x, k_y)$  at each  $(k_x, k_y)$ . The PEAD patterns for binding energies from -1.0 to 10 eV are taken with intervals of 0.2 eV. Figure 23 gives the bird-

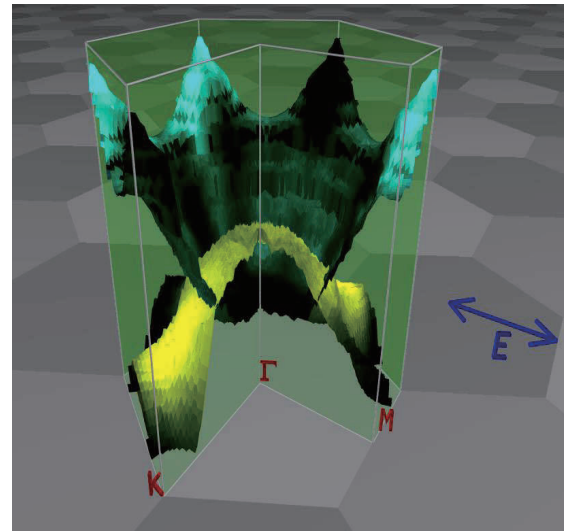


**Fig. 23** Bird's eye-stereo view of 3 D  $\pi$ (green) and  $\sigma$ (yellow) bands of graphite. Photon Energy of 37.5 eV was used for excitation. Vertical scale is the binding energy from 10 eV(bottom) to -1.0 eV(top). Courtesy of Prof. Takizawa.

eye stereo view of the 3-D band dispersion surfaces of graphite [32]. The bright areas are where the original photoemission intensity is high. The first BZ of graphite is indicated as a green hexagonal prism with one-fourth of its volume being cut away to indicate the  $\Gamma$ -K and  $\Gamma$ -M directions. The top of the prism corresponds to the Fermi level and the bottom to the binding energy of 10 eV. The patches of the hexagonal tiles underneath stand for the other BZ's. The 3D shape of the  $\pi$  band dispersion such as the saddle-like feature at the M points or vertices at the K-points is easily recognized. The  $\sigma$  band dispersion colored yellow has a maximum at the  $\Gamma$  point and saddle-like features at the M points. These band dispersion “surfaces” contain fruitful information compared with the conventional band dispersion “curves” along a certain direction in the  $k$ -space. The atomic orbitals composing each band can be determined from 2-D photoelectron intensity distribution. Further, the angular dependence of the slope (velocity) and the curvature (mass) of local band structure can be derived. The integrated band energy over entire BZ, which can be regarded as the electronic part of the condensation energy, could also be obtained.

### (4) 1-D surface states on a stepped metal surface

By slanted cutting of a Ni(111) single crystal, we can obtain the Ni(332) stepped surface, as shown in Fig.24. Angle resolved photoemission spectra (ARPES) at the photon energy of 10 eV give band dispersions of the valence bands. A series of the spectra in the left figure are those obtained by angle scan perpendicular to the stepped line, while those in the right figure are by

angle scan along the stepped line. The peak at the threshold can be attributed to the surface state mainly come from stepped atoms. This was confirmed by gas exposure, which reduced the feature. Interestingly, a distinct band dispersion is found in the right figure, but not in the left figure. This result indicates that strong interaction occurs along the stepped atoms, but not perpendicular to the stepped line. Even though the sample is metal, stepped atoms have quite localized 1-D character along the stepped line. Prof. Namba has conducted these ARPES works at BL-8, aiming for the fundamental understanding of the electronic structure of metal surfaces [33,34].

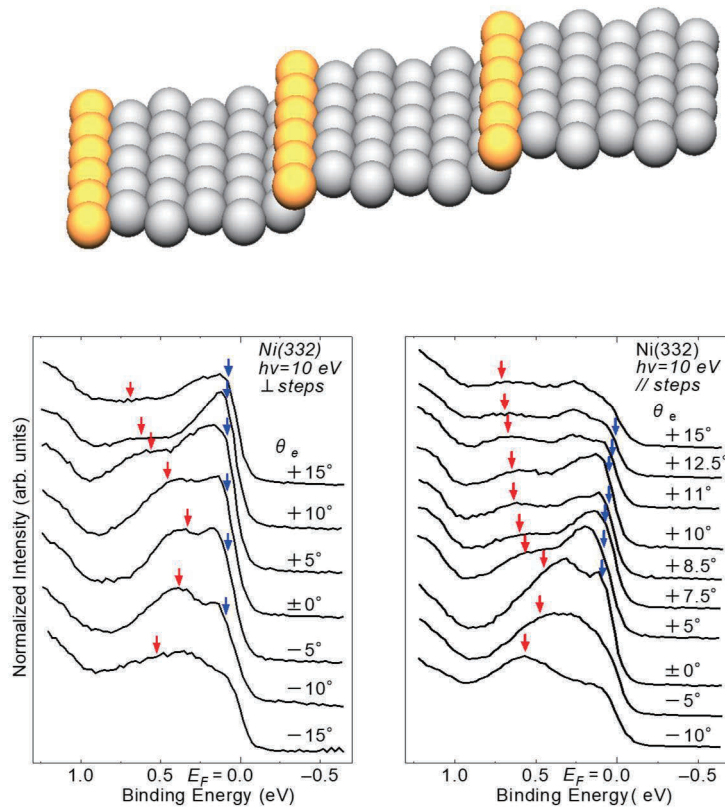


**Fig. 24.** Top: schematic model of Ni(332) stepped surface [33]. Bottom left; ARPES spectra scanned perpendicular to the stepped line. Bottom right: those scanned along the stepped line. Red arrows are band dispersion of the terrace surface and blue arrows are that of stepped surface.

### (5) Soft X-ray XAFS studies

XAFS is one of the most popular methods of synchrotron radiation applications. In the SR center, there were several beamlines for XAFS experiments, such as BL-2,4,8 and 10, which were actively used by outside scientists not only from academia, but also from industries, making use of the nanotechnology supporting program. Among the XAFS experiments performed in the center, two subjects should be picked up. One is the XAFS studies of Li compounds, which are in general unstable and easily oxidized. J. Tsuji and Prof. Taniguchi of Osaka Electro-

Communication University studied the XAFS spectra of several Li compounds, as well as Li metal with the aid of DV- $X\alpha$  calculations [35,36]. Although the spectral qualities were not always good, they are cited even at present as pioneering works.

Another is the XAFS studies of liquid crystals and some oriented polymers performed by Prof. Namba's group at BL-8 in collaboration with Japan Synthetic Rubbers Co. Ltd. An interesting example is the application to photo-induced dimerization of considerably large and complex monomer units, PMI-15, which is a side chain of a polymer, functioning as the liquid crystal alignment [37]. Photo-dimerization reaction of PMI-15 is induced by the irradiation of linearly polarized near ultraviolet (LPNUV) light ( $\sim 36.5$  eV), as schematically shown in Fig. 25. Observed C K-edge XAFS spectra of PMI-15 before and after irradiation is shown as upper spectra in Fig. 26. Although PMI-15 itself is too large and complicated molecule to simulate C 1s core excitation spectra, the 'building block approach' can be applied, which sums up the simulated spectra calculated for subunits of the polymer. In fact, it worked quite well, as shown in the lower simulated spectra in Fig. 26. This work demonstrated that the XAFS method is a very effective for understanding molecular structures and structural changes of complicated functional organic materials.

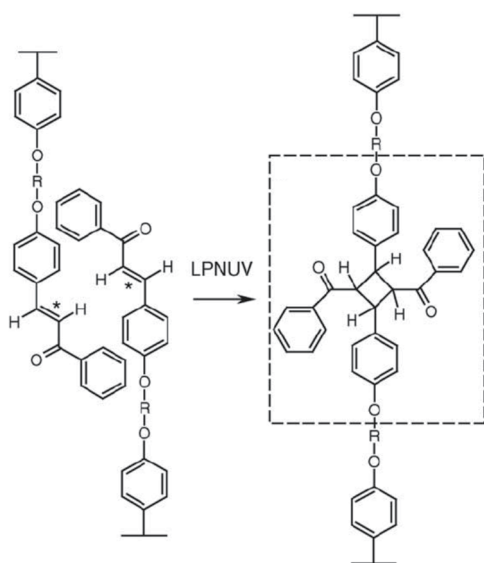


**Fig. 25.** Molecular structure of PMI-15 and the photo-dimerization reaction. Functional groups surrounded by the dashed square are decomposed into several subunits for theoretical calculations.[37]

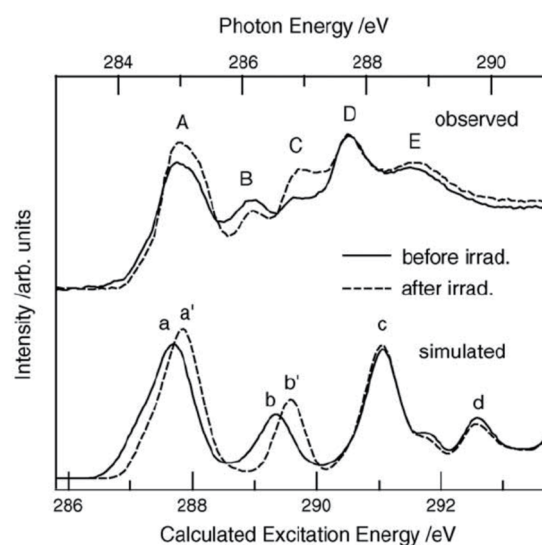


**Fig. 26.** Observed (upper) and simulated (lower) C K-XAFS spectra of PMI. Solid and dashed lines represent the spectra before and after LPNUV irradiation, respectively. [37]

## 1.6 Summary of Phase I

As described above, a private university, Ritsumeikan, had made a great decision to purchase an extraordinary expensive facility. Furthermore, the running cost was not negligible. It was an urgent business how to get funds from the government and industries to cover the running cost. Although it took several years, the SR center succeeded in being one of the facilities for the nanotechnology supporting project in 2002. It was a five years program and had contributed not only to activate the SR researches, especially those related to nanotechnology and nanoscience, but also to help improving several beamlines. In Phase I, the most brilliant scientific activity might be the fabrication of micromachines and micromodules with the LIGA technique. The storage ring, AURORA was designed as the light source for X-ray lithography, and 'LIGA', deep lithography is best matched to the AURORA. Fundamental techniques had been established and many pioneering works had been produced in the field of micromachining. The project of micro- and nano-machining techniques using synchrotron radiation promoted by Prof. Sugiyama (Fig. 27) was selected as the 21<sup>st</sup> COE program by MEXT in 2002. Furthermore, he won the Minister Prize of MEXT for his contribution to the micro-machining technique in 2004.

The LIGA technique is certainly a unique method of fabricating micromachines by making use of the unique feature of synchrotron radiation. However, to make the LIGA a profitable business is other issue. Due to very limited applications, the LIGA project has gradually lost its power and deviated from the main stream. In a sense, it might be a good chance to shut down the SR center. Otherwise, the center had to look for other scientific applications to survive.

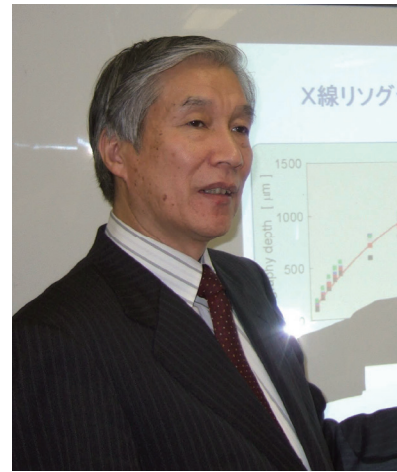


**Fig.27.** Prof. Susumu Sugiyama in his plenary talk of JSR2008, held in Ritsumeikan University, in Jan. 10th, 2008.

## 2. Phase II.

### 2.1 Status of synchrotron radiation facilities in Japan in 2006

In 1996, when the SR center was established, there were only limited synchrotron radiation facilities in Japan; Photon Factory in KEK, UVSOR in IMS and TERAS in ETL. However, in the next ten years from 1996, four facilities have been constructed and started operation. The world biggest SR facility, SPring-8 was constructed in 1997 at Nishi-Harima Technopolis in Hyogo prefecture. This is the third high brilliant hard X-ray light source, following ESRF in Grenoble (1994) and APS in Chicago (1996). At the same site of SPring-8, another compact ring, New SUBARU was constructed as a subsidiary of University of Hyogo. Hiroshima Synchrotron Radiation Center, HiSOR was constructed in 1997 in the Higashi-Hiroshima campus, again as a subsidiary of Hiroshima University. In 2005, Kyushu synchrotron radiation center (Saga Light Source) was constructed at Tosu in Saga prefecture. HiSOR is exclusively for academic use, while New SUBARU and Saga Light Source are more oriented to industrial applications. SPring-8 has also a mission to encourage industrial uses. Surprisingly, 4 facilities have been constructed and operated in those ten years. Figure 28 shows synchrotron radiation facilities existing in Japan in 2006. Synchrotron radiation has been proved to be an indispensable tool in materials science and life science, and attracted many industries.



**Fig. 28.** Synchrotron Radiation facilities operated in Japan in 2006. In each yellow box, (top) facility name, (middle) ring energy, and (bottom) circumference of the ring and the year established in parenthesis.

## 2.2 Status of the beamlines in the SR center

Figure 29 shows the beamline layout of the center in 2006. The LIGA project was still active and four beamlines (BL-5,6,14 and 15) were operated for it. BL-5 and 6 were conducted by Prof. Sugiyama, but Prof. Tabata, another leader of LIGA moved to Kyoto University and his beamlines (BL-13 and 15) turned to be non-used. XRD beamline (BL-1) was originally constructed by Prof. Iwasaki and succeeded by Prof. Nakamura. BL-2, equipped with an old-fashioned soft X-ray monochromator was managed by Prof. Kojima, and XAFS beamlines (BL-3 and 4) were managed by Prof.

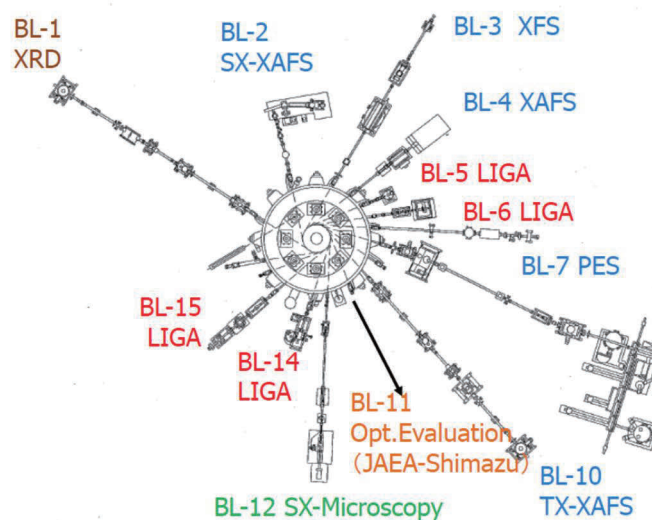


**Fig. 29.** Beamline layout of the SR center in 2006. SX and TX stand for soft and tender X-rays, respectively. SORIS stands for SOR and Ion Scattering.

Ozutsumi. BL-7, equipped with DIANA was managed by Prof. Namba and Prof. Daimon of Nara Institute of Technology. SORIS beamline (BL-8) was managed by Profs. Kido and Namba. BL-11 was rented to JAEA Kansai Institute and Shimadzu Co. Ltd., constructed for evaluation of optical elements. Soft X-ray microscopy beamline (BL-12) was managed by Prof. Namba and Prof. Kihara of Kansai Medical College. Different from other facilities, each beamline belongs to a specific professor except BL-10, of which Prof. Iwasaki used to be in charge. These beamlines were regarded as a kind of extended branches of research laboratories and the management of each beamline was not under control of the director. Professors in charge of beamlines enjoyed extraterritorial privilege and rights.

## 2.3 Assignment of the director of SR center

Prof. Okamoto was expected to step down the director of SR center in Fiscal 2005. Then, I was nominated to be the successor, since I just retired the professorship of the University of Tokyo in March, 2006. I used to be deeply involved in the Photon Factory project since its planning stage and to be a beamline staff in charge of soft X-ray beamlines and an intensive user of the Photon Factory after moving to Hiroshima University and later to the Univ. Tokyo. I have ever worked in design and construction of a soft X-ray double crystal monochromator beamline, VUV Seya-Namioka beamline, and two grazing incidence monochromator beamlines equipped with varied line space plane gratings in Photon Factory. When I visited Ritsumeikan University before the

contract, Prof. Kawamura, vice-President of the University told me the issues requested, which were to ‘activate’ the center, and to get big funds from the government for further development. However, my research field so far was surface science, studies of atomic, electronic and magnetic structures of molecules on metal surfaces by using PES, surface XAFS, and XMCD methods. These experiments in UHV atmosphere were almost impossible in the center! I decided to jump into a quite new field, throwing away my research subjects so far. The situation of the center was worse than I expected. The light source AURORA is a previous generation ring, not appropriate for spectroscopic studies. Many more advanced facilities exist in Japan, as shown in Fig. 28. Thus, the budget request for any advanced research project at the SR center must be very difficult. To make matters worse, more than 15 years have passed since the AURORA ring was constructed and any serious trouble might happen at any time. Especially, the use of superconducting magnet needs extra care for the maintenance. For the worst case, the ring would be shut down without recovery. The directorship was a three years contract. Since the post was not based on the faculties, I could concentrate myself on the matters of the center, but I was not confident of responding the requests by Prof. Kawamura in the three years at all. Anyway, the arrival of a newcomer might be expected to renew the blood of the center.

## 2.4 Management of the SR center

The SR center is a belonging of Research Organization of Science and Technology in Ritsumeikan University. According to the bylaws of the center, important matters are decided by the steering committee, consisting of the director, professors in charge of beamlines, technical manager in charge of the accelerators and consultants. Dean of the faculty of science and technology, Director of the Research Organization and Secretary general were also members, but had not attended the meeting at all since 2006.

In a sense, the head of the university did not place high importance on the center anymore. It means that we could not expect any support from the university for future development. However, from another point of view, it was happy to be able to manage the center without any interference from the head of the university.

I asked Prof. Namba to be a sub-director. He served as a liaison between SR center and faculties until his retirement in 2016. Without his efforts, I could not manage the center smoothly.

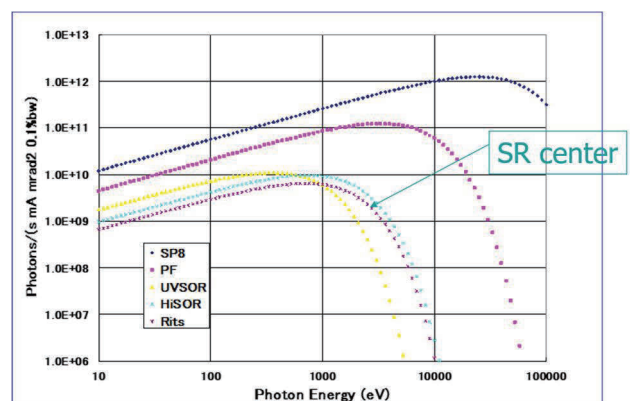


**Fig. 30.** Photon energy distributions of the photon flux from bending magnet from several Japanese SR facilities.

My mission was to ‘activate’ the center by getting funds and constructing new beamlines without interfering with existing beamlines and producing scientific outputs. It was not easy to make the light source comparable with other SR facilities in Japan. Figure 30 shows the photon flux distributions from bending magnet for these existing facilities in Japan. In the AUROLA ring, we cannot increase the electron energy any more, since the applied magnetic field has been maximized up to saturation. Thus, we have no chance to win SPring-8 and PF in the hard X-ray region, while there is no big difference of photon fluxes in the lower energy region. Especially, in the infrared region, total photon flux is determined by the product of the ring current and acceptable solid angle, nothing to do with the electron energy. Therefore, by making full use of the features of the compact ring, we would be able to prepare a beamline with higher performance than SPring-8. Thus, I planned to develop a high photon flux infrared beamline. Although the acceptance angle of the SR beam port is limited to  $30 \text{ mrad}^{\text{H}} \times 30 \text{ mrad}^{\text{V}}$ , insertion of mirrors to focus the light source point makes us possible to increase the acceptance angle substantially, as schematically shown in Fig. 31. This is the idea similar to MIRRORCLE designed by Prof. Yamada. Since the reflectance of a mirror in the infrared region is almost 100 %, multiple mirror system would provide us a very intense infrared beamline. I planned to perform the infrared microscopy experiment with the spatial resolution of  $5 \mu\text{m}$  at  $2000 \text{ cm}^{-1}$  (diffraction limit). In order to overcome the limit, I further planned to install the near field optics and aim the spatial resolution of submicron. Fortunately, JST (Japanese Science and Technology Agency) publicly invited applications for ‘Regional funds to foster research project’. Important condition for the application was to get a patent in advance. Thanks to an excellent help of the Research Office, the patent was smoothly accepted [38] and the joint proposal with TRC (Toray Research Center), entitled “Development of high-performance infrared micro-spectrometry for bio- and medical usage” was fortunately approved as a three years project by JST in 2007. This was the first step for the revolution of the SR center.

Final goal in my mind then was to establish the center for characterization of materials with every possible photon energy using synchrotron radiation. In 2007, Dr. Iwao Watanabe joined in

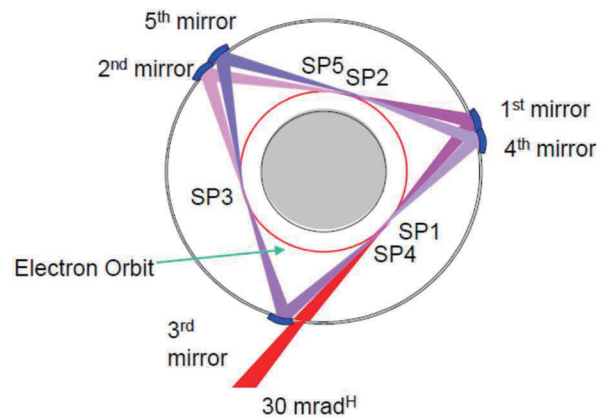


**Fig. 31.** Possible idea of a high photon flux Infrared beamline. The aperture of the SR port is  $30 \text{ mrad}^{\text{H}}$  and usually, we use the beam emitted from the source point SP1, but by installing the 1<sup>st</sup> mirror, we can collect the beam at SP2. Further, by installing the 2<sup>nd</sup>, 3<sup>rd</sup> and 4<sup>th</sup> mirrors, photon flux would be increased with the number of mirrors, since the IR reflectivity is almost 100% [38].

the center. He used to be an old friend of mine and has been specialized in XAFS. Since then, he has been a reliable adviser and collaborator for the upcoming development of the beamlines.

In 2008, Prof. Shin Imada moved in Faculty of science and technology from Osaka University and in 2009, Prof. Yasuhiro Inada moved in Faculty of life science from Photon Factory. Both were active researchers of synchrotron radiation science and quite helpful for the development of the center, as described later.

Nanotechnology supporting program funded by MEXT ceased in fiscal 2006, but nanotechnology network project started from fiscal 2007 as the subsequent program. Fortunately, the SR center was approved to join the project, together with SPring-8. Thus, we could continue to support users and to cover the fees of beamline staffs, although the budget was reduced to 1/3 of the previous project. It continued up to 2011 (5 years support). Instead, another program to support industrial use, named “Open Advanced Research Facilities Initiative”(先端研究施設共用促進事業) chose our center as one of advanced research facilities, which had been working from 2009 to 2015. Since supporting budget from MEXT decreased year by year, we had to look for other funds.

Fortunately, in 2009, a very big national project for developing secondary batteries started in NEDO, conducted by Prof. Ogumi of Kyoto University. It was called “RISING”(Research & Development Initiative for Scientific Innovation of New Generation Batteries), whose basic concept was to develop new batteries with high performance, based on the characterization of mechanisms of batteries by making full use of the most advanced methods, such as synchrotron radiation, neutron, and NMR, as well as theoretical simulations. In the synchrotron radiation field, SPring-8 has the highest performance for hard X-rays, but not for soft X-rays. Then, the SR center was chosen as a branch station in charge of soft X-ray XAFS experiments. It was a seven years project with plenty of budget, sufficient for supporting fees of four beamline staffs and improving beamlines. Subsequent program, “RISING2” had worked from 2017 to 2021 and the further program, “RISING3” has been working since 2021 as a three years program. Without support from the RISING project, management of the SR center would be very difficult.

After retirement of Prof. Namba in 2015, I asked Prof. Inada to be a sub-director. He has greatly contributed to the RISING project by developing imaging XAFS beamlines, in addition to the work as a liaison between the SR center and faculties.

## 2.5 Development of beamlines

Since I started the directorship of the center, I had devoted myself to scrap old-fashioned spectroscopy beamlines and build new ones or replace with newer ones which had not been used in other facilities.

### (1) Soft X-ray XAFS beamline (BL-2)

A friend of mine in NTT informed me that a soft X-ray beamline fell into disuse since the SR facility ‘ALIS’ in NTT Atsugi Laboratory shut down the operation. I visited Atsugi Laboratory and found it available in our center without changing any optics. The beamline was constructed by Shimadzu Co. Ltd, 10 years before, equipped with a Hettrick mount monochromator with three kinds of varied line spacing gratings, covering the energy from 40 to 650 eV. The whole system was carried in the center in February, 2008 and settled down at the BL-2, where the old beamline had been removed. We were lucky to use the beamline as it was, although it was necessary to clean all optical components by using the UV-ozone asher and to install an encoder system for energy calibration. Dr. Watanabe conducted all the works and made the beamline available in March, 2009. Figure 32 is a photo of Dr. Watanabe examining the performance of the beamline. By adding one more grating, available energy extended up to 1000 eV. The optical layout is schematically shown in Fig. 33. In 2011, a sample chamber was fabricated for XAFS experiments, equipped with a wide aperture (effective area of 80 mm<sup>2</sup>) SDD (Silicon drift detector), whose energy resolution was 80 eV at 600 eV, as shown in Fig. 34. Mn L-XAFS spectrum of MnO<sub>2</sub> taken with the PFY (Partial Fluorescence Yield) mode, using the SDD is compared with that taken with the TFY (total fluorescence yield) mode, using an MCP with a



**Fig. 32.** Dr. Watanabe was examining the performance of the installed beamline, BL-2 in March, 2009.

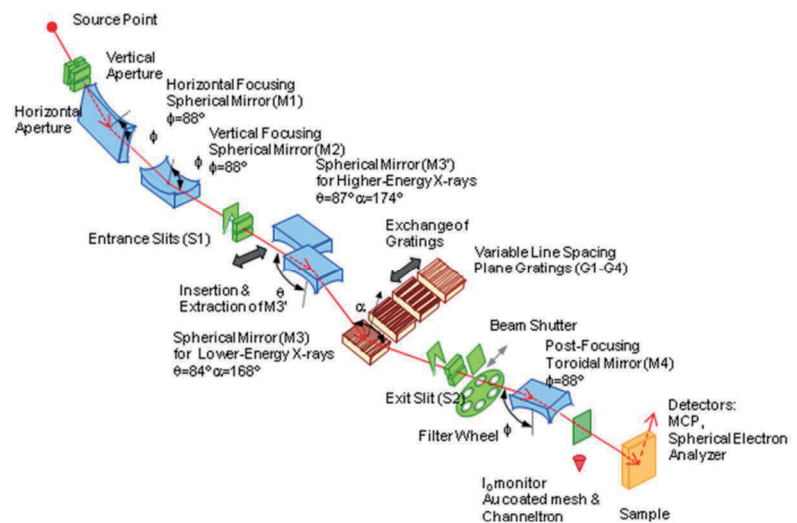


**Fig. 33.** Schematic diagram of BL-2. Four kinds of gratings are exchangeable to cover the energy from 50 to 1000 eV.

Dr. Watanabe conducted all the works and made the beamline available in March, 2009. Figure 32 is a photo of Dr. Watanabe examining the performance of the beamline. By adding one more grating, available energy extended up to 1000 eV. The optical layout is schematically shown in Fig. 33. In 2011, a sample chamber was fabricated for XAFS experiments, equipped with a wide aperture (effective area of 80 mm<sup>2</sup>) SDD (Silicon drift detector), whose energy resolution was 80 eV at 600 eV, as shown in Fig. 34. Mn L-XAFS spectrum of MnO<sub>2</sub> taken with the PFY (Partial Fluorescence Yield) mode, using the SDD is compared with that taken with the TFY (total fluorescence yield) mode, using an MCP with a

reverse retarding bias. This demonstrates how effective the PFY mode is, as shown in Fig. 35. This beamline has been actively used for characterization of secondary batteries.

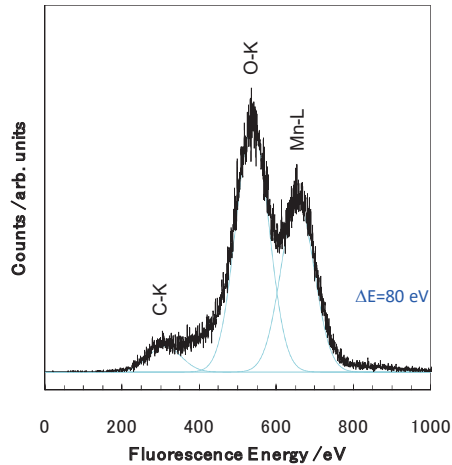


**Fig.34.** X-ray fluorescence spectrum from  $\text{Li}_2\text{MnO}_3$ , taken with the newly installed SDD. Mn L emission was well separated from O K, indicating the high energy resolution ( $\Delta E=80$  eV).

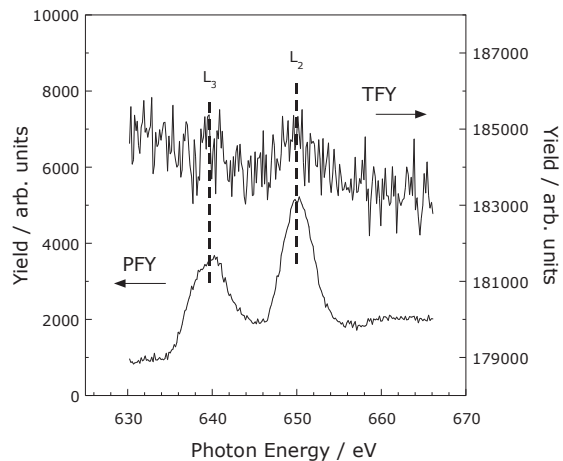


**Fig. 35.** Mn L-XAFS spectrum from  $\text{Li}_2\text{MnO}_3$  with the PFY mode, compared with that with the TFY modes whose background is very high.

## (2) Infrared Micro-spectrometry (BL-15)

As described above, we succeeded in getting the fund for constructing an infrared micro-spectrometry. However, to construct the beamline, we had to open the vacuum chamber of the storage ring and install mirrors. It was not an easy task! In April, 2007, we had a chance to open the chamber and found it difficult to insert many mirrors surrounding the electron orbit because there were so many obstacles inside the chamber to hamper the beam path. As a result of it, we had to change the optical design completely. The optical system finally decided consisted of one toroidal mirror and two plane mirrors, accepting the SR beam of  $250 \text{ mrad}^{\text{H}} \times 60 \text{ mrad}^{\text{V}}$  solid angle. This was still much higher than the IR beamlines existed in the world. Installing these three mirrors in the ring chamber was really a tough work, because (1) the space allowed for the mirrors was very limited, (2) cooling was necessary to protect the X-ray beam at the central part of the electron orbit plane, (3) a remote control system for fine adjustment mechanism was necessary for the toroidal mirror, (4) all the components installed should be non-magnetic, since the chamber was in the superconducting magnet, (5) once the optical system was installed, we could not change or modify the system, since reopening the chamber costs fortune and takes at least one week. The mirror system installed in the ring chamber is shown in Fig. 36. The beam taken out from the ring was reshaped into a parallel beam by using a parabolic mirror and introduced in Nicolet6700 (Thermo Co. Ltd.) and ContinuumXL, as shown in Fig. 37.

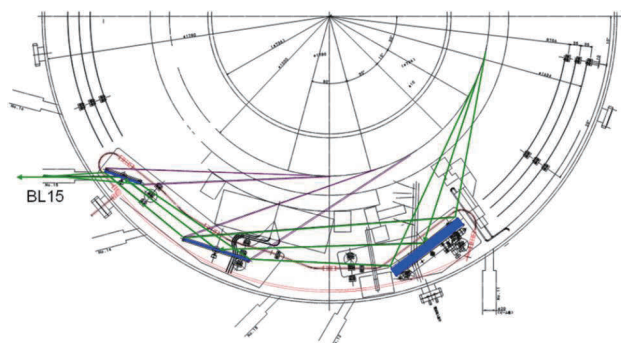


**Fig. 36.** The mirror system installed in the ring chamber. Blue: mirrors, red: cooling pipes, Green: IR rays. The first toroidal mirror was tuned by using an UHV compatible non-magnetic pico-motor.



**Fig. 37.** Infrared Spectro-microscopy beamline (BL-15). Center: FT-IR (Nicolet 6700) and left: Microscopy (Continuum XL).

The performance test of the beamline, in comparison with that of laboratory source, revealed that SR based IR is much superior to the laboratory source for IR microscopy due to its high brilliance [39]. Spatial resolution is roughly  $5 \mu\text{m}$  at  $1000 \text{ cm}^{-1}$ . Thus, we can get an IR spectrum of a specific area with  $5 \mu\text{m}$  resolution and also a mapping of a specific functional group. Figure 38 shows a typical example applied for human cancer cells. This beamline was constructed in March, 2010 and has been used mostly for bio-medical studies [40-44].

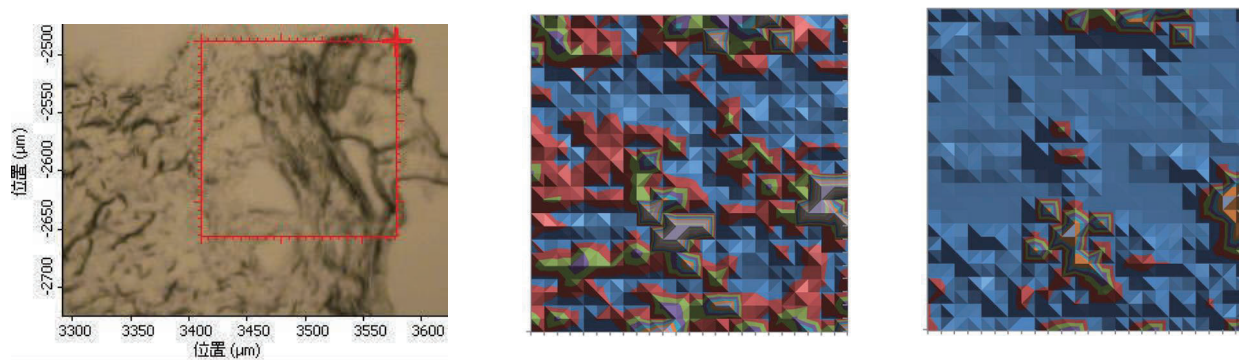


**Fig. 38.** Images of human cancer cells. (Left) Image of the optical microscopy. Red square has a size of  $170 \times 170 \mu\text{m}^2$ . (Middle) Map of the P=O group, which distributes over the cancer cells. (Right) Map of the C=O group, indicating spots of necrosis. Courtesy of Dr. Miyoshi of Fukui Univ.

### (3) VUV spectroscopy beamline (BL-1)

Recently, there are few beamlines for VUV spectroscopy in Japan, possibly due to lack of needs. Spectro-chemistry center, Univ. Tokyo possessed a VUV beamline, equipped with Seya-Namioka type monochromator in Photon Factory (BL-7A), but nobody used it any more. In fact, this

beamline was designed and constructed by me when I was a beamline staff of PF and by negotiation with the spectro-chemistry center, I succeeded in inheriting the monochromator. BL-1 was used for XRD, but was closed after retirement of Prof. Nakamura. Thus, it was scrapped and reborn as a VUV beamline. Prof. Imada is in charge of this beamline. Originally, ARPES experiments were planned, but were given up due to strong magnetic field from the superconducting magnet. However, this beamline is available for absorption and/or reflectivity experiments in the VUV region [45].

#### (4) Tender X-ray XAFS beamline (BL-10)

BL-10 is a tender X-ray beamline consisting of a pre-focusing toroidal mirror, a Golovchenko-type double crystal monochromator, constructed in 1997. Five kinds of crystal pairs were prepared: KTP(110), Beryl(10 $\bar{1}$ 0), InSb(111), Si(111) and Ge(111), covering the energy from 1000 to 4000 eV. Some demonstrative experiments had been done before, but any publishable work had not been produced yet. Several improvements were performed at this station, such as installation of multi detection modes and an extra chamber for the experiment in atmospheric pressure.

In the soft and tender X-ray regions, TEY, PEY and PFY detection modes are quite common for XAFS experiments, in which the penetration depth of X-rays is relatively short. Simultaneous use of these three modes provides a useful depth profiling method: PFY is bulk sensitive, while TEY is surface sensitive, and PEY is more surface sensitive. The PEY mode is generally performed by the set of a retarding grid and an MCP. If we use the conventional setup, it works successfully in the low energy soft X-ray region below 1000 eV, but it does not work above

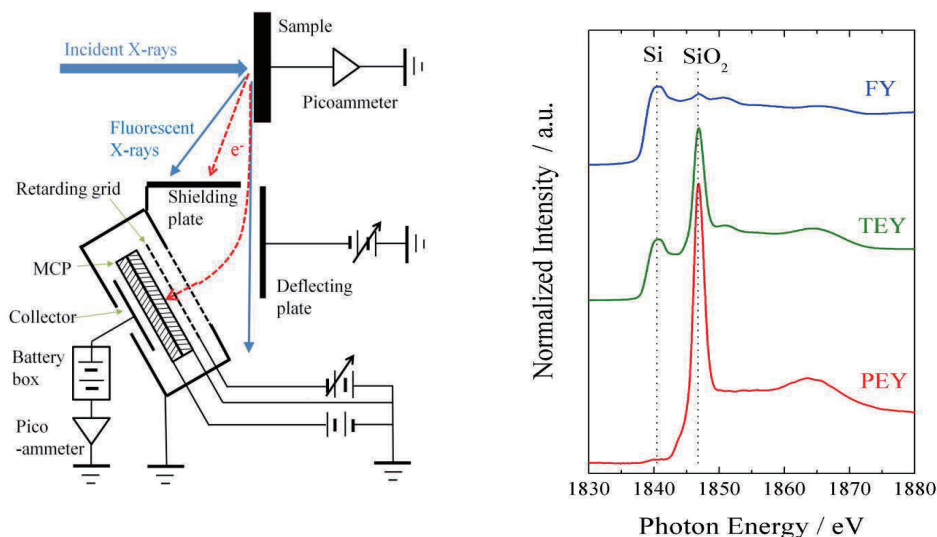


**Fig. 39.** (left) Experimental setup for the PEY mode for tender X-ray XAFS, in which only electrons come into a MCP. (right) Si *K*-XANES spectra of a Si crystal covered by 8 nm thick oxide, taken with FY, TEY and PEY modes[46].

1000 eV due to mixing of FY spectra. We developed a FY free PEY system, whose setup is shown in Fig. 39 (left). A demonstrative example is shown for a silicon crystal covered with silicon oxide in Fig. 39(right), where the surface sensitive PEY gives exclusively a spectrum of SiO<sub>2</sub>, while PFY with SDD gives that of bulk Si and TEY monitored with leak current gives a spectrum intermediate between Si and SiO<sub>2</sub>.

According to the strong request of users, we developed a compact sample transfer system from a glove box to a sample chamber without exposing to air. Figure 40 shows a compact transfer vessel, in which a sample rack with 8 sample plates can be loaded. We checked how long the pressure was sufficiently low after sealing and confirmed that the dew point temperature was kept under -80 °C for more than 24 hours. We made this sample transfer system available for all the XAFS beamlines.

We also developed a cell for liquid samples. Due to the low penetration depth of soft and tender X-rays, to find a thin and vacuum-tight X-ray window is essential. We found SiN<sub>x</sub> and polyimide thin films were available in the tender X-ray region. Furthermore, incorporation of electrodes in the cell has made *in situ* XAFS possible. We have developed a special cell for the operando analysis of XAFS. Here, a typical electrochemical cell is shown in Fig. 41, which has worked successfully for the operando Si, P and S K-XAFS experiments [47]. As a demonstrative experiment, P K- operando XAFS was measured for the charging process of LiFePO<sub>4</sub>, as shown in Fig. 42. Although the spectral change is much less significant than that of Fe K-XAFS, appearance of the pre-edge peak indicates the growth of FePO<sub>4</sub>.

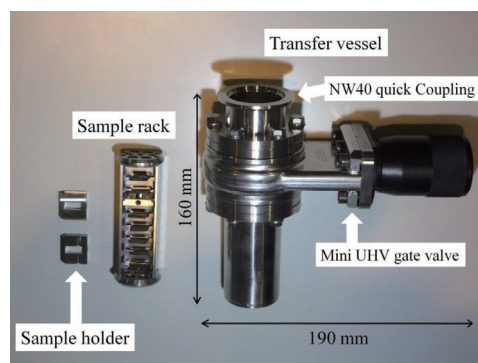


Fig. 40. A compact sample transfer vessel.

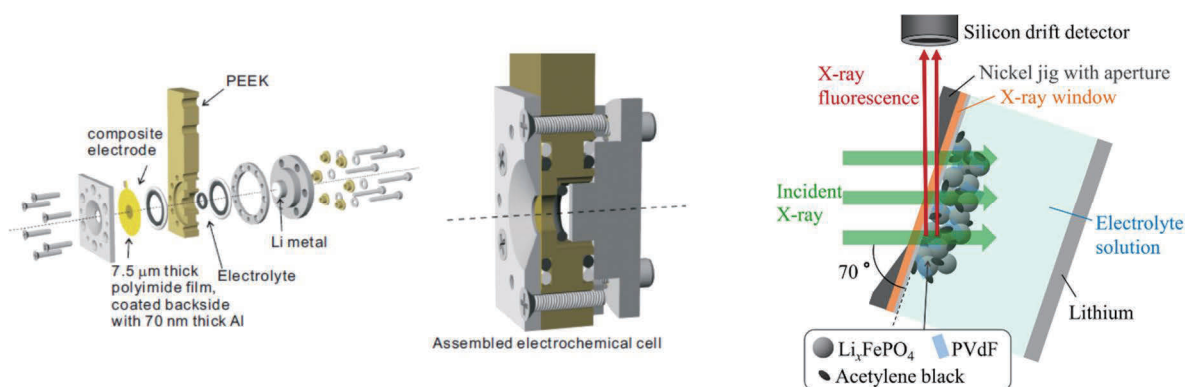
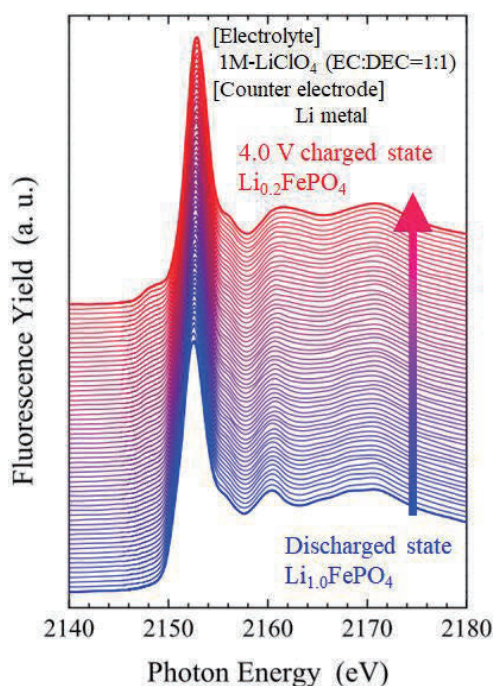


Fig. 41. An electrochemical cell for operando XAFS experiment in the tender X-ray region, developed in our center. 7.5 μm thick vacuum tight polyimide film was used as an X-ray window. Reprinted with permission from Ref. 47. Copyright [2014], AIP Publishing LLC.



**Fig. 42.** Operando P K-XAFS spectra of  $\text{LiFePO}_4$  in the charging process from 3.2 V to 4.0 V in 200 min. Each spectrum was taken in 3 min. Reprinted with permission from Ref.47. Copyright [2014], AIP Publishing LLC.

### (5) Soft X-ray XAFS beamline (BL-11)

Although the soft X-ray XAFS (BL-2) beamline was actively used, it had several essential problems. Ground floor of the center was not robust. Especially, the site of BL-2 was close to the compressor pumps for Liq. He cryo-cooling, whose vibrations were propagated to the monochromator via the floor and caused to deteriorate the energy resolution, especially in the higher energy. The space around the sample chamber was so narrow that it was difficult to extend experiments. Furthermore, the optical system was not fully optimized and lost fair amount of photon flux. Thus, a new beamline for the soft X-ray region was strongly desired. In 2013, MEXT generously distributed the budget for improving beamlines to the SR facilities joining in the program, “Open Advanced Research Facilities Initiative”. Fortunately, we got a sufficient budget to construct a new sort X-ray beamline. BL-11 was robust without vibration source nearby, which was originally used by Shimadzu and JAEA, shut down in 2008. Then, it was replaced with a new beamline in 2013~2014. I asked Prof. K. Amemiya (KEK-PF) for a basic design of the optics and gratings and Dr. Watanabe again for construction of the new beamline. Figure 43 shows the beamline layout of BL-11. Since we designed the beamline, based on the optical ray tracing, the performance of BL-11 is much superior to BL-2. Three kinds of varied line space plane gratings are exchangeable, covering the energy from 50 to 1000 eV.

Ni L-edge XAFS spectra from NiO taken at BL-11 were compared with that at BL-2 in Fig. 44. Note that the more the groove density of the grating is and the narrower the slit width is, the higher the energy resolution is. Although the grating in BL-11 was not same as that in BL-2, Fig. 44 clearly indicates higher performance of BL-11 than BL-2.

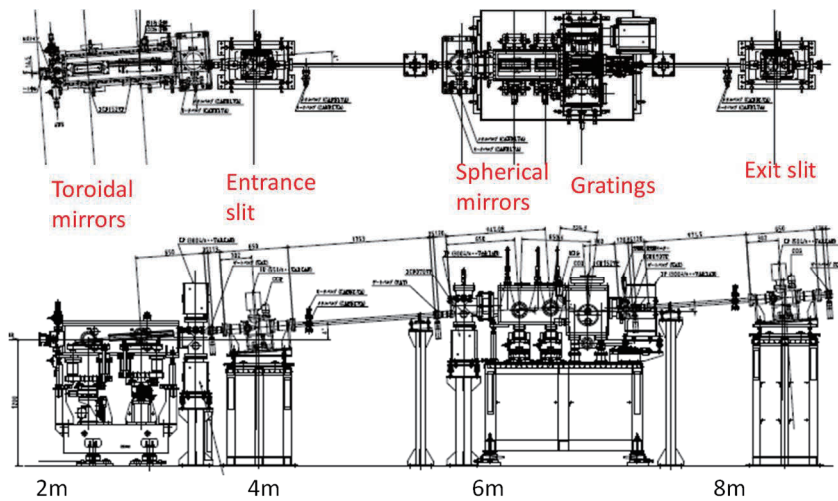


**Fig. 43.** Newly constructed soft X-ray XAFS beamline (BL-11). Upper: Plan view, and lower: side view. Distance is from the source point.

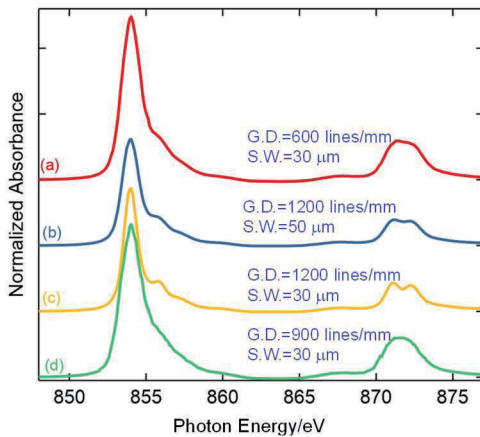


**Fig. 44.** Ni L-edge XAFS spectra from NiO taken at BL-11 (a), (b), and (c), compared with that at BL-2 (d). G.D. is the groove density and S.W. is the slit width.

As described above, operando XAFS has been performed successfully in the tender X-ray region, However, we found it impossible to use the same cell in the soft X-ray region, because the window was too thick to make X-rays pass into a sample in this energy region. We must find a very thin, transferrable, but vacuum-tight film. Recently, all-solid-state batteries have been developed using polymer and/or ceramic ion conductive sheets. They are regarded as promising rechargeable batteries with greater safety and higher energy density. Operando XAFS experiment might be applicable for the all-solid-state batteries, since it is not necessary to care for liquid leakage in a vacuum chamber. As a model all-solid-state cell, we adopted a  $\text{Li}^+$  conductive glass ceramic (LICGC) solid electrolyte sheet,  $\text{Li}_2\text{O}-\text{Al}_2\text{O}_3-\text{SiO}_2-\text{P}_2\text{O}_5-\text{TiO}_2-\text{GeO}_2$ , which generated self-formed anode inside of the solid electrolyte. As a cathode,  $\text{LiMn}_2\text{O}_4$  was chosen with several thicknesses from 50 nm to 500 nm. The cell structure thus prepared and experimental setup are shown in Fig. 45. Operando soft XAS measurements were performed continuously during charging process in the constant current mode up to the cut-off voltage of 2.2 V. It took about 25

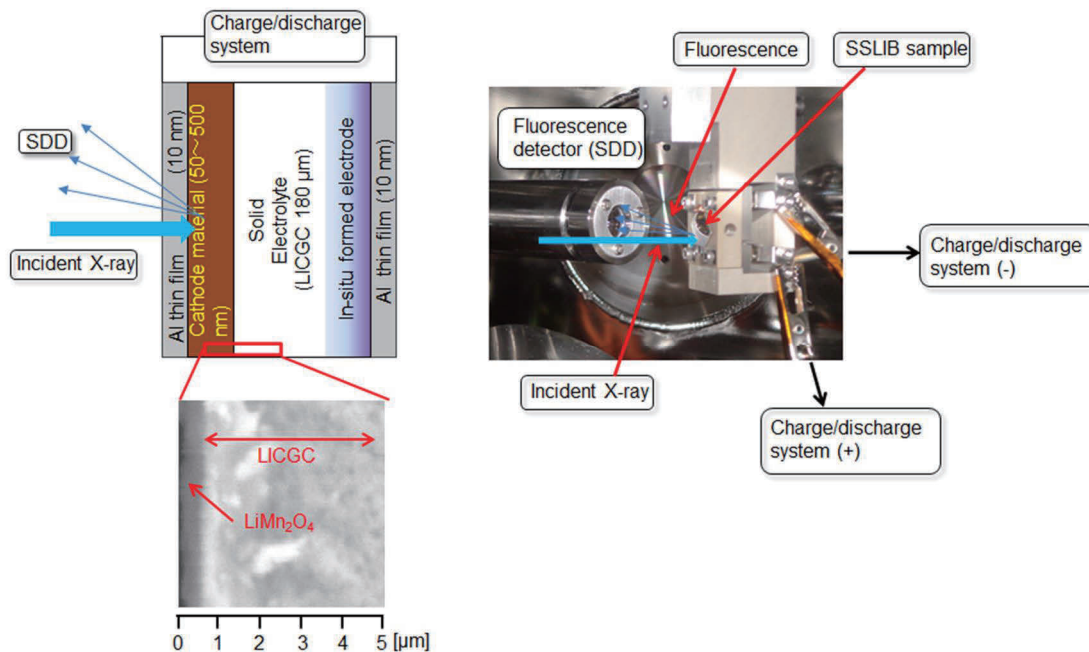


**Fig.45.** (Left) Constitution of the all-solid-state battery. 10nm thick Al was coated on both side of the cell as an electrode. SEM image of a part of the cathode and LICG is also shown below. (Right) Photo of the home-made assembly for in situ and operando experiments installed in a XAS chamber [48].

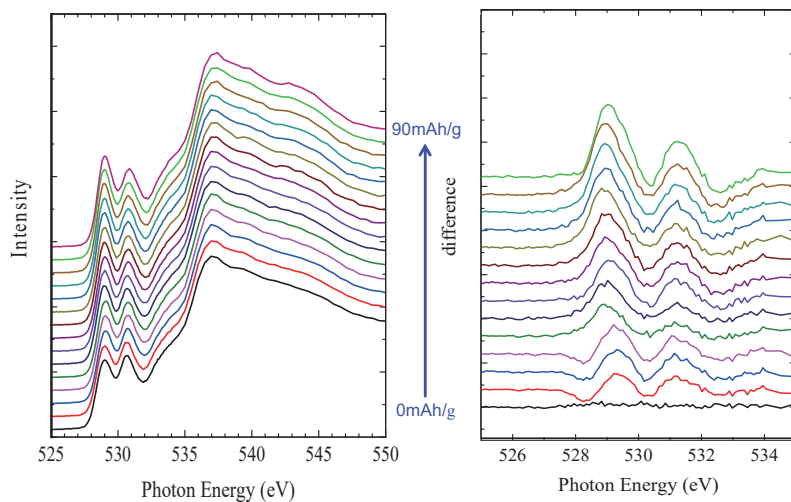


**Fig. 46.** Evolution of O K-XAFS spectra with charge. (Left) raw spectra. (right) spectra subtracted from that before charge. Thickness of the cathode was 50 nm [48].

min. to obtain a spectrum in the energy region from 515 to 665 eV covering both O K-edge and Mn L-edge, and about 12 min. for a Ti L-edge spectrum from 435 to 530 eV. Figure 46 shows the evolution of O K-XAFS spectra with charge. Although spectral difference was very small, spectra subtracted from that before charge (right figure) clearly indicate the increase of two peaks at 529 and 531 eV with charge, whose peaks are associated with charge transfer from O 2p to Mn 3d to keep charge balance. This experiment demonstrated a potential of in situ and operando soft XAS measurements for detailed analyses of all-solid-state batteries [48], which won the best paper award from Electrochemistry in 2018.

**(6) Tender X-ray XAFS beamline (BL-13)**

BL-10, tender X-ray double crystal beamline was so crowded that one more beamline was needed, which covered from 1000 to possibly 5000 eV. We decided to prepare for it from the NEDO RISING budget, although the total amount was very limited. For the construction of the new beamline, special care was paid for the high energy resolution and beam size at the focal point. A set of parabolic mirrors is generally adopted to make a parallel beam for high resolution. However, it costs fortune and takes more than one year to fabricate parabolic mirrors. We proposed to use two toroidal mirrors, one for producing a parallel beam and another for focusing the beam at the sample position [49]. Although a set of two toroidal mirrors is not ideal to produce a parallel beam, the ray-tracing simulation clearly indicates that the quasi-parabolic toroidal mirror (1:∞ focusing) produces a nearly parallel beam comparable with a parabolic mirror. Another quasi-parabolic toroidal mirror (∞:1) focuses the beam at the sample position in a size of 1 mm<sup>H</sup> x 1 mm<sup>V</sup>. The results of ray tracing are shown in Fig. 47, clearly indicating that quasi-parabolic toroidal mirror is sufficient for our purpose. The beamline layout constructed at BL-13 is shown in Fig. 48, indicating that the total length from the source point to a sample chamber is only 7 m! This is another advantage of adopting the parallel beam optics, since we can make the beamline either longer or shorter. BL-13 was constructed in

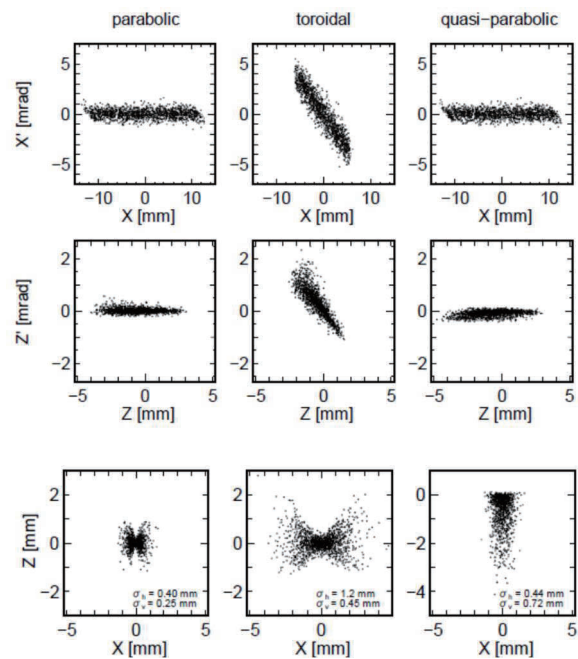


**Fig.47.** Top: Phase space diagram of the SR beam (8 mrad<sup>H</sup> × 2 mrad<sup>V</sup>) at the monochromator position for parabolic mirror, 1:1 focusing toroidal mirror and quasi-parabolic (1:∞ focusing toroidal) mirror. x and x' denote position and dispersion in the horizontal direction. Middle: Phase space diagram for z and z', denoting the position and dispersion in the vertical direction. Bottom: The beam profiles at the focal point.

2013 -2014 and several performance tests revealed higher resolution and higher intensity than BL-10 [50]. Si K-edge XAFS spectrum of c-Si taken at BL-13 was compared with that at BL-10, as shown in Fig. 49. Doublet structure at the absorption edge is clearly observed in the spectrum of BL-13 and the standing wave profile appeared around 1976 eV exhibits much higher resolution in BL-13 than in BL-10.

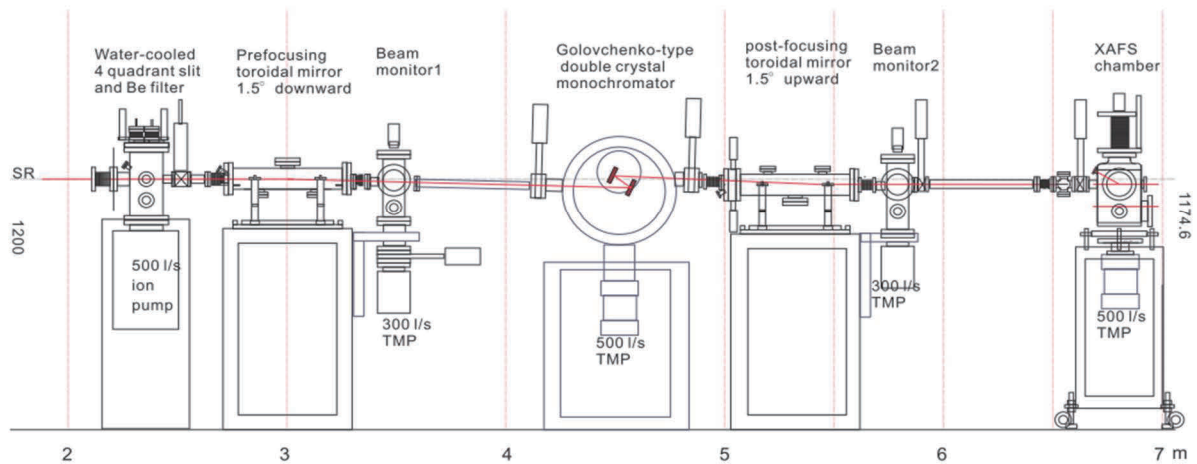


**Fig. 48.** Beamline layout of BL-13, tender X-ray beamline, equipped with a double crystal monochromator and two quasi-parabolic mirrors. Beam is deflected downward by  $1.2^\circ$  and shaped in quasi-parallel beam. Monochromatized beam is deflected upward by  $1.2^\circ$  and focused at the focal point, 7m apart from the source point.

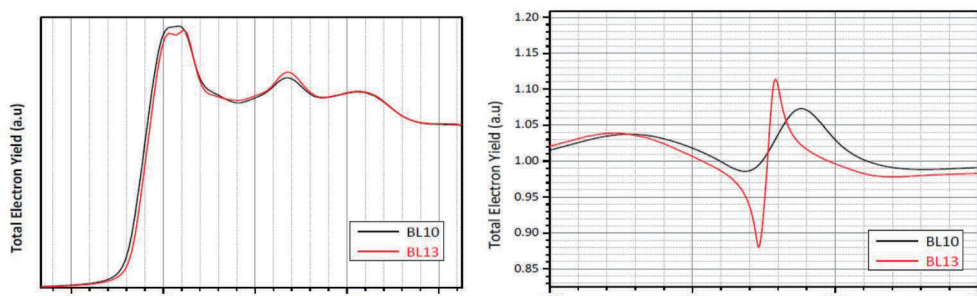


**Fig. 49.** Si K-edge XAFS spectra of c-Si obtained at BL-13(red line) and at BL-10(black line). Left: XANES region of c Si, Right: Standing wave profile generated from Si(111) diffraction.

**(7) Imaging XAFS beamline (BL-4)**

BL-4 was a conventional XAFS beamline, consisting of  $I_0$  ion chamber, Golovchenko-type double crystal monochromator and  $I$  ion chamber. It had been used for XAFS experiments in Phase I. However, the AURORA is a low energy ring, not appropriate for hard X-ray experiments. Prof. Inada modified this beamline for imaging XAFS, first introducing a linear photodiode array [51], later c-MOS 2-D detector [52], as shown in Fig. 50. Of course, there are several “imaging XAFS “ beamlines in Japan. For example, SPring-8 has one, whose detecting area is less than  $100 \mu\text{m}^2$ . It is useful to examine microstructures, but cannot apply to soft materials due to high photon density. In contrast, imaging XAFS at BL-4 irradiates samples in rather wide area with moderate

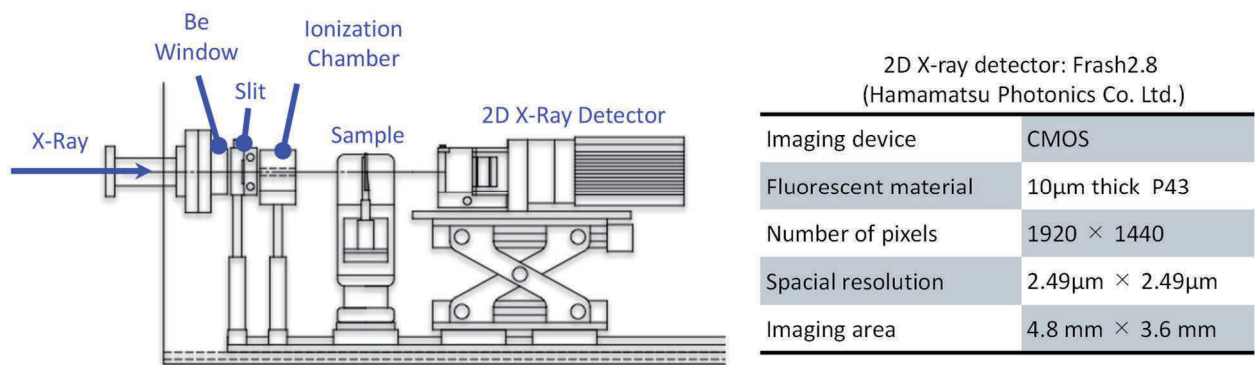


**Fig. 50.** Layout of the imaging XAFS at BL-4, where 2D X-ray detector is Frash2.8 developed by Hamamatsu Photonics, Inc. Ltd. The performances are listed in the right table. [52]

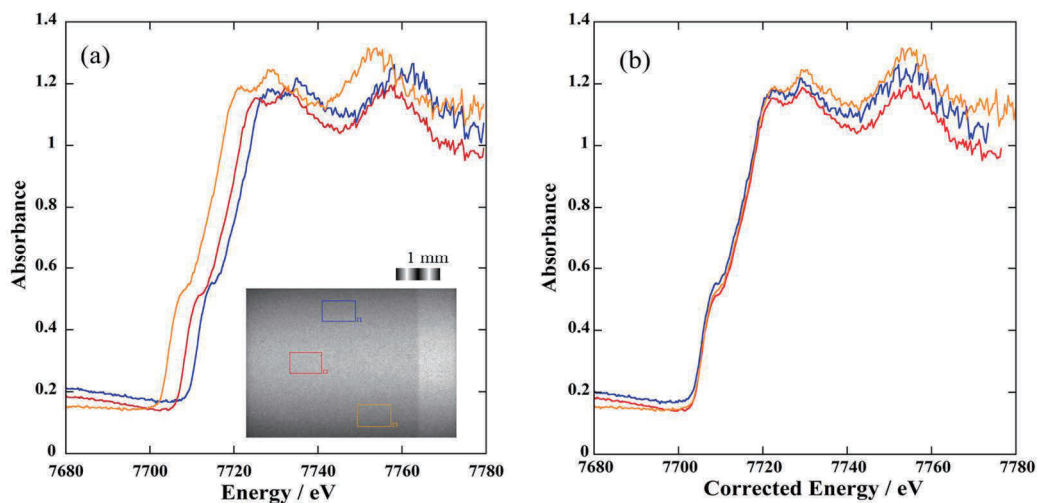


**Fig.51.** Co K-edge XANES spectra of Co foil. (a) Spectra at different vertical positions and (b) Spectra, energy corrected by the vertical position [53].

photon density, especially useful for examining soft materials, such as batteries, as described later.

Another advantage of adopting a 2D detector is to improve the energy resolution. Figure 51(a) shows Co K-edge XAFS of Co foil by using a 2D detector [53]. Edge energy shifts with the vertical position, since the photon energy disperses along the vertical direction. The higher the vertical position is, the higher the photon energy is. Thus, we can get the spectrum with higher energy resolution by correcting the energy shift at the vertical position on the detector, as shown in Fig. 51(b).

Typical application of the imaging XAFS technique was for lithium ion batteries. It was applied to the study of charging process of a  $\text{LiFePO}_4$  electrode [54]. In the charging process, electrochemical reaction takes places as follows.



Fe K-edge imaging XAFS experiment was performed and a spatial distribution of  $\text{Fe}^{2+}$  (discharged state) and  $\text{Fe}^{3+}$  (charged state) of in the charging process in the 2 mm x 2 mm size was obtained, as shown in Fig. 52.

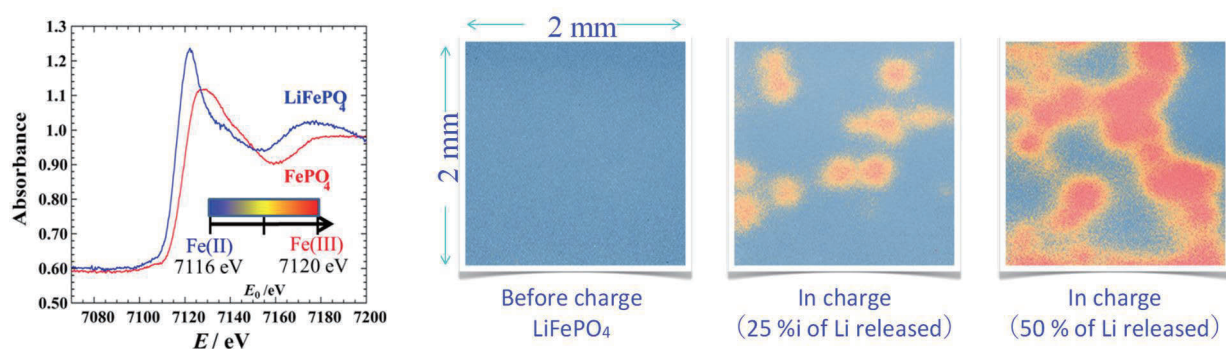


**Fig.52** (Left) Fe K-XANES spectra of  $\text{LiFePO}_4$  (discharged state: blue) and  $\text{FePO}_4$  (charged state: red). Color changes from blue to red by oxidation. (Right)  $\text{Fe}^{2+}/\text{Fe}^{3+}$  ion distribution in the charging process. At a site, where  $\text{Li}^+$  is removed,  $\text{Fe}^{2+}$  changes to  $\text{Fe}^{3+}$ . Thus, Fe oxidation is a marker how  $\text{Li}^+$  is removed.

A distinct non-uniform charging was so clearly observed, which gave a big impact to battery society, since it provided useful information about the charge/discharge mechanisms of secondary batteries. This inhomogeneity indicates the existence of low resistant reaction channels. To investigate the origin of the reaction channels, effects of cell thickness, mixing ratio of active material, acetylene black and PVDF, and the porosity (vacancy ratio) should be examined.

### (8) Vertically Dispersive XAFS beamline (BL-5)

The 2D imaging XAFS is a very effective tool to get spatial distribution of reaction paths, but it takes too much time to trace the reaction distribution in the operando condition. In 2013, Prof. Inada and Dr. Katayama designed and constructed a new unique method to obtain quick 1D

imaging XAFS at BL-5, which used to be a LIGA beamline. This is a combination of the imaging XAFS and wavelength dispersive XAFS (DXAFS) techniques, where the former is in the horizontal direction and the latter is in the vertical one. This is a new method to obtain both space-resolved and time-resolved XAFS [55]. Prof. Inada named this method ‘VDXAFS (Vertically Dispersive XAFS)’, whose schematic layout and experimental setup is shown in Fig. 53. The rectangular-shaped white X-ray beam is vertically diffracted by a cylindrical polychromator. Because the incident angle of the X-ray to the polychromator crystal changes along the curved surface, the diffracted X-ray energy is dispersed in the vertical direction. The utilization of a 2D detector enables the spatial resolution in the horizontal axis of the incident X-ray beam, which makes it possible to perform the sequential measurements of the XAFS data array and to analyze the dynamic change of inhomogeneous electrode reactions of LIBs during the charge and discharge processes. Typical application of the VDXAFS is again to the charge and discharge processes of  $\text{LiFePO}_4$ . Figure 54 shows how charge and discharge processes propagate with time. Charge/discharge rate changes at each position, causing preferential reaction channels. Interestingly, a position at which charge proceeds quickly, discharge process proceeds quickly.

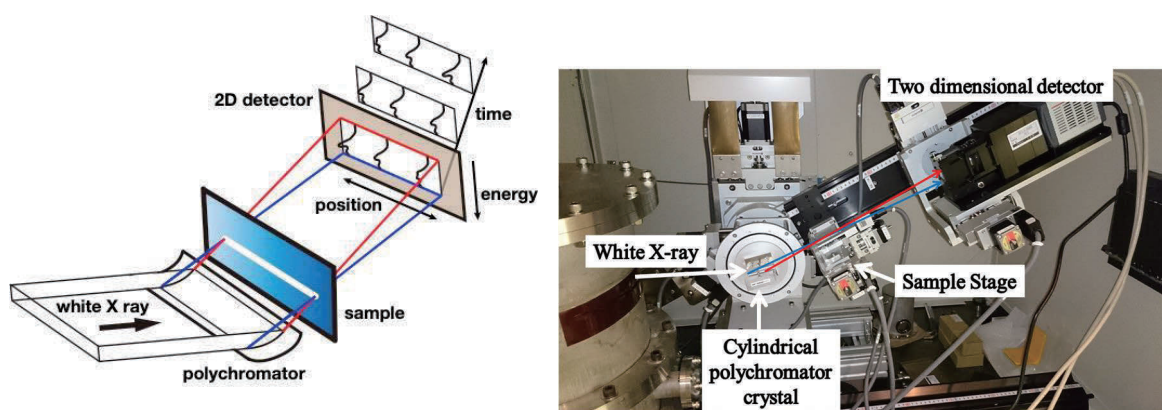


**Fig.53.** (Left) Schematic layout of the VDXAFS and (right) a photo of the CDXAFS setup [55].

The incident beam with the size of  $4 \text{ mm(V)} \times 10 \text{ mm(H)}$  is focused as a line-shape beam, and the electrode sample is placed at the focal position. The transmitted and vertically dispersed X-ray intensities are detected using the CMOS type 2D detector (ORCA-Flash 4.0, Hamamatsu Photonics). The detector has  $2048 \times 2048$  pixels and the element size is  $6.5 \mu\text{m} \times 6.5 \mu\text{m}$ . The polychromator crystal is placed on the  $\theta$  stage, and the sample and the detector are installed on the  $2\theta$  stage. A Si (111) crystal with 0.5 mm thickness is used as the cylindrical polychromator, and the crystal is held on a holder which has a fixed concave curvature with the radius of 1 m.

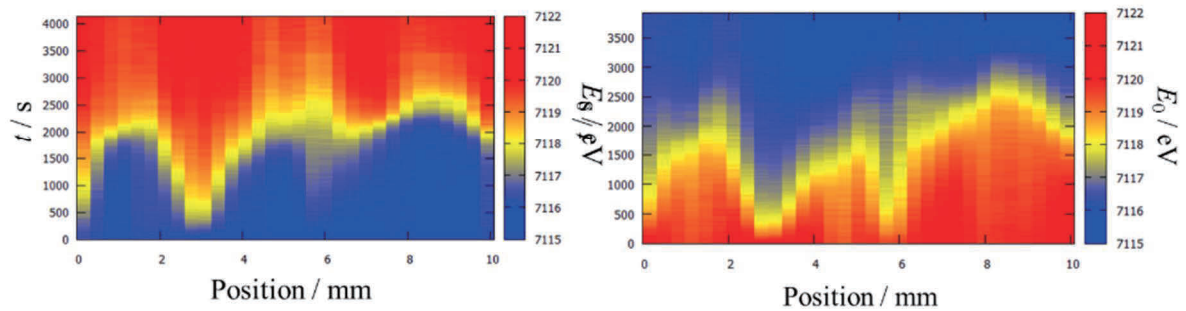


**Fig. 54.** Evolution of the charge (left) and discharge (right) processes of  $\text{LiFePO}_4 \leftrightarrow \text{FePO}_4$ , observed at a 10 mm wide rectangular position of the electrode with the VDXAFS method. Charge/discharge rate changes at each position.

### (9) Double elements DXAFS (BL-5)

Dispersive XAFS (DXAFS) method is one of the advanced techniques of XAFS, which gets a XAFS spectrum simultaneously. DXAFS has been actively applied for the study of time-resolved structural changes, but it gives the structural information around only one element. Prof. Inada's group extended this DXAFS to monitor double elements simultaneously, by using two polychromators and a wide-range position-sensitive detector [56]. Schematic layout of this method is shown in Fig. 55 for the case of Ni and Mn K-XAFS from  $\text{LiNi}_{1/3}\text{Co}_{1/3}\text{Mn}_{1/3}\text{O}_2$ . The experimental setup was loaded at BL-5, exchanging with the VDXAFS setup. This method is useful to monitor structural changes of multi-elements simultaneously.

### (10) Beamline layout in 2018

As described above, old beamlines were scrapped and new beamlines were constructed one after another, thanks to the support by MEXT and NEDO (the RISING project). As shown in Fig. 56, the beamline layout has changed drastically from that in 2006 (Fig. 29). They are mostly spectroscopic beamlines, covering the energy range from infrared to hard X-rays. Barriers between beamlines, which existed in 2006, were taken away and all the beamlines turned to be open to any users. Thus, the SR center has been reborn as a center for characterization of functional materials by synchrotron radiation spectroscopies.

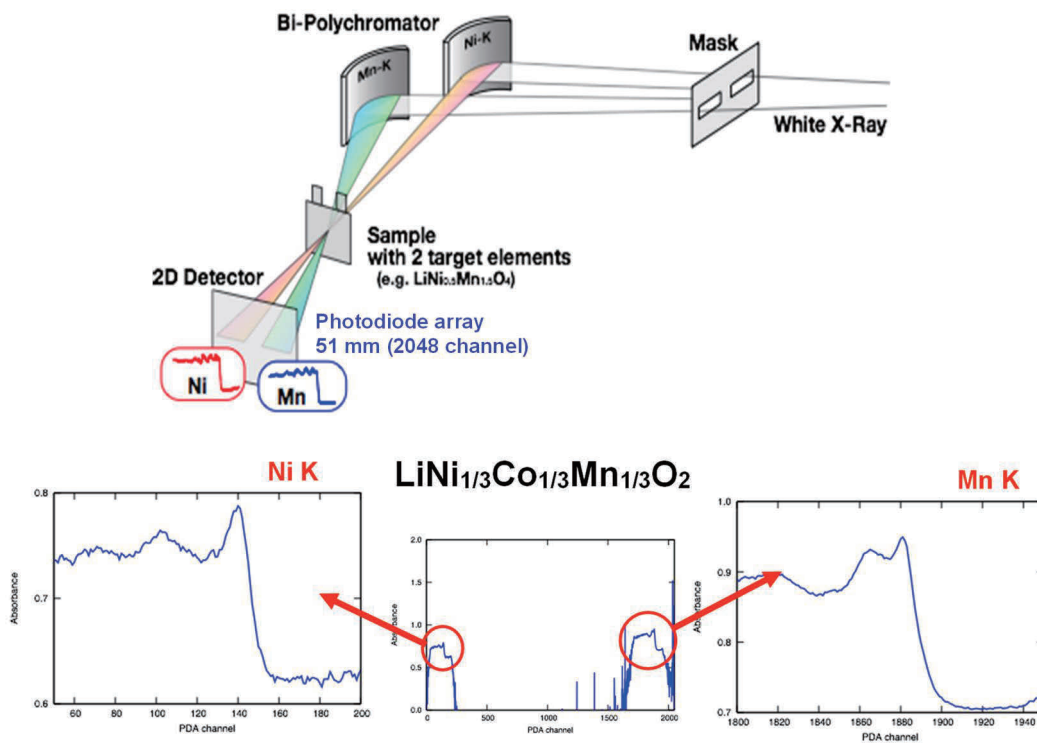


**Fig.55.** (top) Schematic layout of the Double Element DXAFS method [56]. At the sample position, the double X-ray beams were focused into 0.38 mm. (Bottom center) Signals on a 51mm long (2048 channels) photodiode array. (Bottom left) Enlarged spectrum of Ni K-XANES, (Bottom right) Enlarged spectrum of Mn K-XANES.

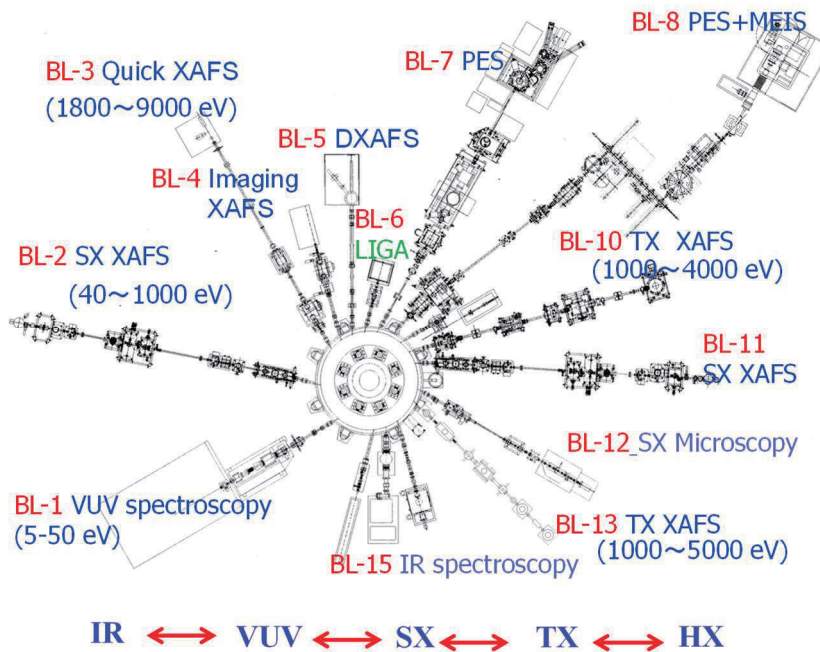


**Fig. 56.** Beamline layout of the SR center in 2018.

## 2.6 Scientific outputs

In Phase II, experimental studies performed at the SR center were oriented to characterization of materials by using spectroscopies. Especially, after joining the RISING project group in 2009, we have developed several techniques, necessary for the studies of secondary batteries and as a result, 90 % of the works were concerned with batteries. A huge earthquake and subsequent incredibly gigantic tsunami happened on March 11<sup>th</sup> in 2011 in Tohoku area, which caused serious disasters in nuclear plants in Fukushima. This accident dramatically changed the policy for energies. Development of alternative clean and safe power sources has been strongly desired. Secondary battery is a representative of clean energy. We accepted many users aiming at the development of secondary batteries with higher performance, not only from academia, but also from industries. Followings are typical scientific outputs of the SR center from 2006 to the present.

### (1) Characterization of Si nanosheets

Dr. Hideyuki Nakano (Fig. 57) and his group in Toyota Central Research Laboratory have succeeded in synthesizing Si nanosheets by adding HCl to CaSi<sub>2</sub> at -30°C in an inert atmosphere and leaving it for 5 days [57]. The Si nanosheets have an enormous potential for a wide range of applications, since Si-H bond can be easily replaced with various kinds of functional groups, as shown in Fig. 58(left). Si K-XAFS was applied to characterize the products. Since the products are air-sensitive, the transfer vessel



**Fig. 57.** Dr. Hideyuki Nakano (Toyota Central Research Laboratory).

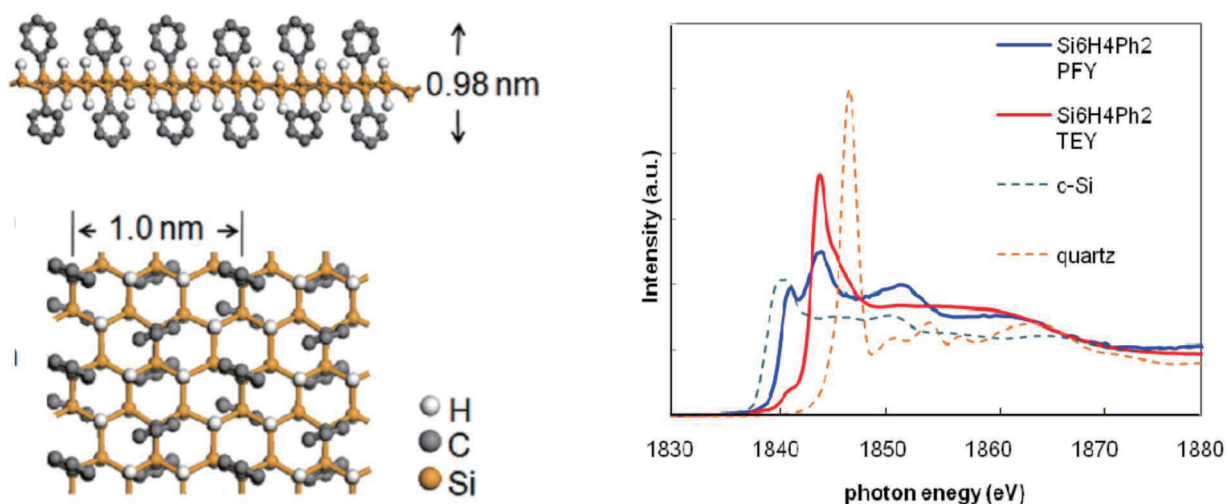


**Fig. 58.** (left) Structural model of a Si nanosheet, substituted with phenyl group. (Right) Si K-XANES spectra of the Si nanosheet (Si<sub>6</sub>H<sub>4</sub>Ph<sub>2</sub>), taken with the TEY and PFY modes, compared with those of c-Si and SiO<sub>2</sub>. Reprinted from Ref. 57. Copyright (2010), American Chemical Society.

was effectively used. The spectra are shown in Fig. 58(right), which clearly indicates that the nanosheets consist of Si-Si and Si-H bonds, but no Si-O bond. They developed nanosheets with several functions and reported the results in high impact journals [58-63], which have been cited by more than 300 papers. In fact, Dr. Nakano has opened the door of the SR center for characterization of functional materials and greatly contributed to the scientific activities of the center.

## (2) Characterization of Li-S batteries

Elemental sulfur is one of the promising cathode active materials for high-energy rechargeable lithium batteries because of its high theoretical capacity (ca. 1670 mAh/g) and relatively low cost. However, this active material has some disadvantages, such as low electronic/ionic conductivity and dissolution as polysulfides into electrolyte during electrochemical cycling (resulting in shuttling of polysulfides), both of which are responsible of limited rate capability and rapid cycle

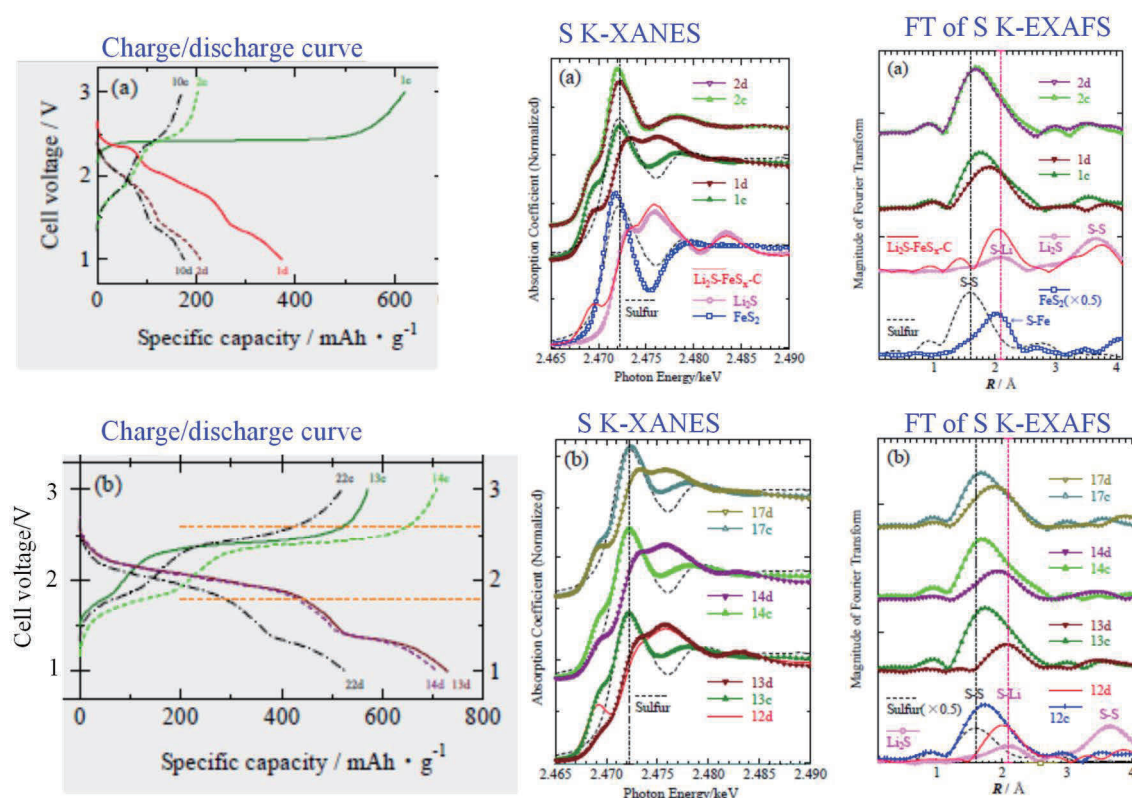


**Fig. 59.** Effect of the pre-cycling treatment for the  $\text{Li}_2\text{S}-\text{FeS}_x\text{-C}$  composite electrode [70]. Upper figures (a) are charge/discharge curves, S K-XAFS spectra and Fourier transformed spectra of S K-EXAFS obtained with the conventional method, and lower figures (b) are those after the step-wise pre-treatment. Charge/discharge curves after pretreatment (b) indicate longer cyclability and higher capacity. S K-XAFS spectra after pre-treatment (b) exhibit that the chemical state of S at charge is different from that at discharge even after 17 cycles, indicating the battery has a longer lifetime. Reprinted from Ref. 70. Copyright (2015), American Chemical Society.

degradation in Li-S cells. Dr. Takeuchi's group in AIST have prepared several types of Li-S cells, forming the composites with carbon powders, using the spark-plasma-sintering (SPS) process, and applied to all-solid-state cells [64-71]. In the process of improving the performance, characterization with XAFS was very useful. As a typical example, Fig. 59 shows the effect of pre-cycling treatment of  $\text{Li}_2\text{S-FeS}_x\text{-C}$  composite electrode to improve the cyclability [70].

### (3) Characterization of Li-O<sub>2</sub> batteries

Li-O<sub>2</sub> battery is known to be one of promising next generation batteries, which provides high specific-energy-density ( $\sim 3 \text{ kWh kg}^{-1}_{\text{cell}}$ ), applied for various portable electronics and electric vehicles in the future. However, the current Li-O<sub>2</sub> battery suffers from huge energy-loss, which arises from the difficulty of decomposition of insulating  $\text{Li}_2\text{O}_2$  on recharge ( $\text{Li}_2\text{O}_2(\text{s}) \rightarrow 2\text{Li}^+ + \text{O}_2(\text{g}) + 2\text{e}^-$ ). Dr. Hye Ryung Byon, a senior researcher in RIKEN (Fig. 60) has studied Li-O<sub>2</sub> batteries to suppress this energy-loss. Her group incorporated metal and metal oxide structures into carbon cathodes in ether-based electrolyte, which could be expected to act as a catalyst to decrease over-potential by the thermodynamically reversible potential (2.96 V vs.  $\text{Li/Li}^+$ ). They studied the charge/recharge processes systematically with XRD, FT-IR, Raman, and TEM, and found that the XAFS technique was quite useful, too. She visited us in the center in August, 2012 and started collaboration with us for characterizing new Li-O<sub>2</sub> batteries. Her group succeeded in suppressing the overpotential by dispersing  $\text{RuO}_2$  NPs (nanoparticles) on the cathode, MWCNTs (Multi Wall Carbon Nanotubes), as shown in Fig. 61. In fact, the recharge voltage reduced from 4.0 V (MWCNTs only) to 3.6 V ( $\text{RuO}_2/\text{MWCNTs}$ ). To clarify the mechanism, we measured O and Li K-XAFS with FY and TEY modes, which provide bulk and surface-sensitive chemical information, respectively. From the spectra with the FY mode (not shown), it turned out that in discharge,  $\text{Li}_2\text{O}_2$  appears on the surface and disappears in recharge. There was almost no difference between with and without  $\text{RuO}_2$  dispersion. In contrast, the TEY



Fig. 60. Dr. Hye Ryung Byon (RIKEN) at the invited talk of the annual meeting of the SR center in June, 2016)

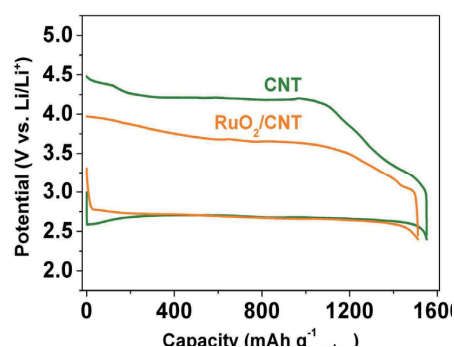
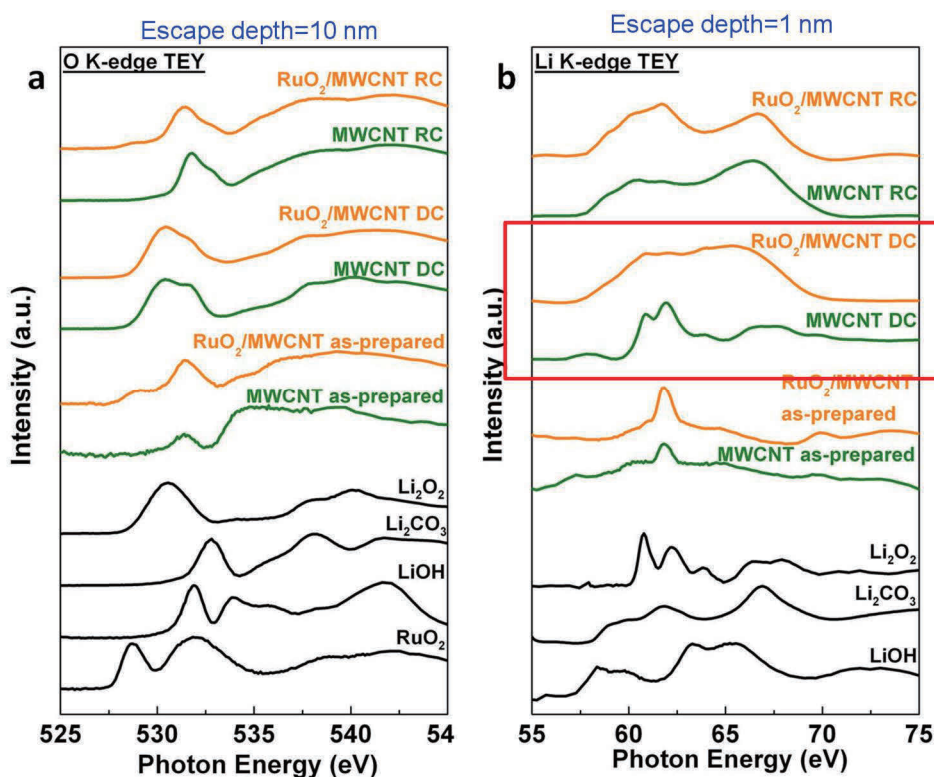


Fig. 61. Electrochemical performance with  $\text{RuO}_2/\text{MWCNT}$  (orange) and MWCNT (green) cathodes at a current rate of  $0.1 \text{ mA cm}^{-2}$  and a discharge cut-off potential of 2.4 V (referenced to  $\text{Li}^+/\text{Li}$ ). Reprinted from Ref. 72. Copyright (2013), ACS Publications.

mode spectra, as shown in Fig. 62, together with several reference compounds, indicate that the Li K-XAFS spectrum at discharge from RuO<sub>2</sub>/MWCNTs is clearly different from that from



**Fig.62.** O K-edge (a) and Li K-edge (b) XANES spectra with the TEY mode of RuO<sub>2</sub>/MWCNT (orange) and MWCNT (green) cathodes as-prepared, 1st-discharged (DC) and 1st-recharged (RC) with references (black) of Li<sub>2</sub>O<sub>2</sub>, Li<sub>2</sub>CO<sub>3</sub>, LiOH and RuO<sub>2</sub>. Spectral difference of Li K-XAFS spectra between with and without RuO<sub>2</sub> at discharge is highlighted by red rectangle. Reprinted from Ref.72. Copyright (2013), ACS Publications.

MWCNTs only, although there is no difference for O K-XAFS spectra. Escape depth of O K-XAFS is about 10 nm, while that of Li-K XAFS might be less than 1 nm. Accordingly, the topmost surface of RuO<sub>2</sub>/MWCNTs is covered by miscellaneous Li compounds, which might be responsible for the higher performance of RuO<sub>2</sub> dispersion on MWCNTs. This work was published in Nano Letters [72], which has been cited by more than 160 papers and once selected to be top 10% of scientific papers. Her group further improved the performance of the Li-O<sub>2</sub> battery and published in many high impact journals [73-78]. In 2016, Dr. Byon moved from RIKEN to KAIST in Korea. She changed main research subject to innovative aqueous lithium-ion batteries and is still collaborating with us [79]. Without doubt, she is one of the great contributors to the scientific activities of the center.

#### (4) Characterization of SEI of secondary batteries

For high cyclability of secondary batteries, SEI (Surface Electrolyte Interphase) is known to play a very important role, but the detailed mechanism is still unknown. Soft X-ray XAFS is very powerful for the study of SEI of batteries. In fact, simultaneous use of PEY, TEY and PFY modes worked very effectively. As described in the previous section, PEY, TEY and PFY modes in the soft X-ray region can probe both surface and bulk structures of batteries. Since deterioration of an electrode usually starts from the surface, XAFS experiment with these three modes provides useful information. We have performed several works relating to SEI in the RISING project [80,81]. Typical example is the application to additives on electrolyte for improving the battery cyclability. We studied the effect of adding lithium bis(oxalate) borate (LiBOB) to the electrolyte on the cyclability of the  $\text{LiCoO}_2$  electrode [80]. Fig. 63 shows O K-XANES spectra of  $\text{LiCoO}_2$  just after soaked and after 20 cycles of charge/discharge with three detection modes. Just after soaked, the surface is covered with  $\text{Li}_2\text{CO}_3$ , though the bulk is predominantly  $\text{LiCoO}_2$ . After 20 cycles, the surface structure does not change in the case with LiBOB, while it changes drastically without LiBOB. From the spectral similarity, we can deduce that the  $\text{LiCoO}_2$  in the surface region decomposed to  $\text{CoO}$ .

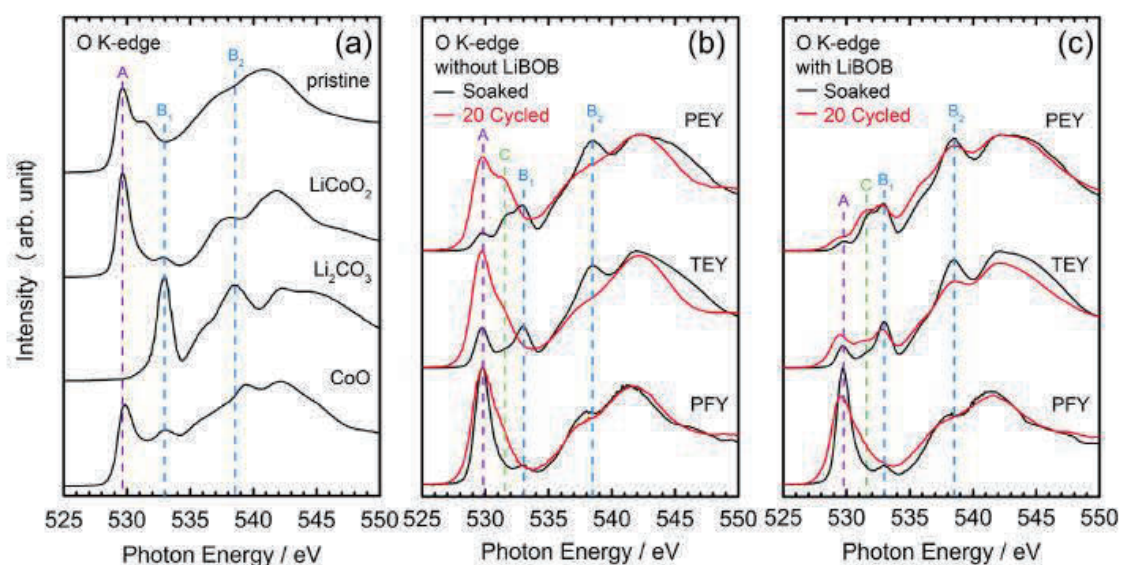


**Fig.63.** O K-edge XANES spectra of the reference compounds: pristine  $\text{LiCoO}_2$ ,  $\text{Li}_2\text{CO}_3$ ,  $\text{CoO}$  powders (a), the soaked and 20 cycled  $\text{LiCoO}_2$  electrode without (b) and with 0.1 wt% LiBOB (c). A, B( $B_1, B_2$ ), C are characteristic peaks of  $\text{LiCoO}_2$ ,  $\text{Li}_2\text{CO}_3$  and organic carbonyl, respectively. Reprinted from Ref.80 with permission of Elsevier.

#### (5) Charge/discharge mechanism of Li-rich batteries

Recently, a series of Li-rich Mn layered oxides,  $y\text{Li}_2\text{MnO}_3 \cdot (1-y)\text{LiMO}_2$  ( $M=\text{Ni}, \text{Co}, \text{Mn}$ ) have been paid a special attention as high capacity positive electrodes in the next generation Li ion batteries [82]. Since such a high capacity cannot be explained only by the redox reaction of

transition metals, oxygen must commit the charge compensation to some extent. Drs. Oishi and Shimoda in the RISING group, in collaboration with us, studied O *K*-edge XANES as well as Ni, Co, and Mn *L*-edge XANES for the  $\text{Li}_{1.16}\text{Ni}_{0.15}\text{Co}_{0.19}\text{Mn}_{0.50}\text{O}_2$  electrode, focusing to the reversible cycles after the initial high irreversible process [83-85]. Fig. 64(a) shows O *K*-edge XANES spectra after 1<sup>st</sup> and 2<sup>nd</sup> fully charged (4.8 V) and discharged (2.0 V) states. The spectra consist of a pre-edge structure (527-534 eV) and a broad structure above 534 eV. The former is associated with the transitions from O 1s to hybridized states of O2p and metal 3d, while the latter with those from O 1s to metal 4s, p and O 2p hybridized states. Upon discharge, double bands at 536 and 540 eV appear. This is a typical feature of the octahedrally-coordinated metal oxides. The peak shift of the main band toward lower energy reflects the metal-O bond lengthening by Li intercalation. Upon charge, the pre-edge peak is enhanced both in the 1<sup>st</sup> and 2<sup>nd</sup> cycles. Fig. 64(b) shows the difference spectra between the charged and discharged states in the pre-edge region for 1<sup>st</sup> and 2<sup>nd</sup> cycles. Peak A1 is due to the formation of the hole state at the charged state, while a newly appeared peak A2 might be associated with peroxide species, whose peak energy coincides with that of  $\text{Li}_2\text{O}_2$  [72]. Although the presence of the peroxide species was proposed by XPS and ESR [86], present experiment is the first direct observation of the peroxide species by O *K*-XAFS.

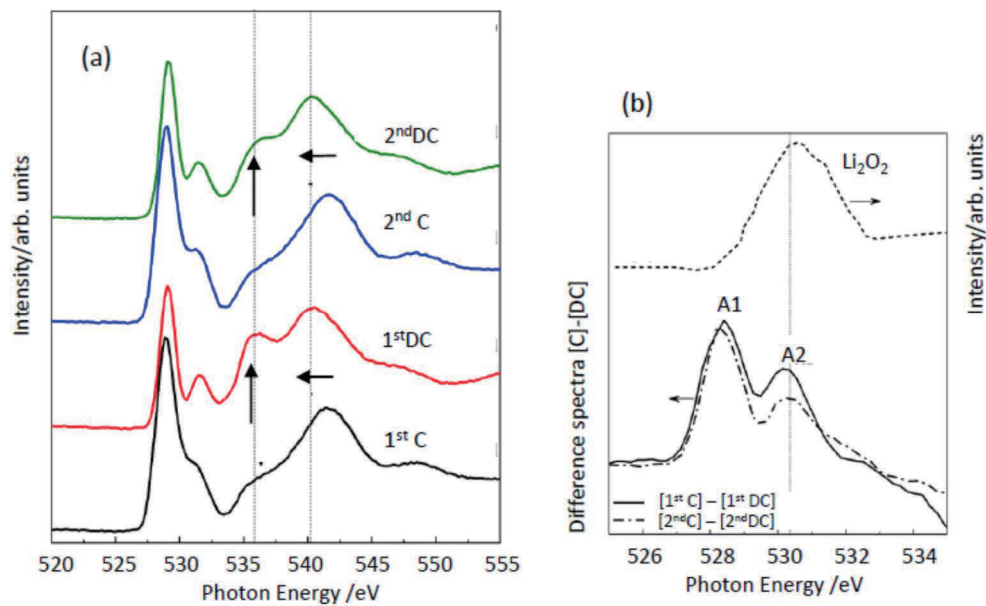


**Fig.64.** O *K*-edge XAFS spectra during the 1<sup>st</sup> and 2<sup>nd</sup> cycles with the TEY mode, in the wide range (a), and the difference spectra between charged and discharged states in the pre-edge region(b). C and DC stand for fully charged and discharged states, respectively. Reprinted from Ref.83 with permission of Elsevier.

## (6) Characterization of innovative secondary batteries

Dr. Naoaki Yabuuchi (Fig. 65) has been actively developing innovative secondary batteries, first in Prof. Komaba's laboratory in Tokyo University of Science, then in 2014 moved to Tokyo Denki University and in 2018 moved to Yokohama National University as a full professor. In 2012, I had a chance to listen to his invited talk about a high-capacity electrode material for rechargeable batteries,  $\text{Li}_2\text{MnO}_3\text{-LiCo}_{1/3}\text{Ni}_{1/3}\text{Mn}_{2/3}\text{O}_2$  [87]. I was impressed in his excellent detailed analysis of the experimental results mainly performed in SPring-8 and after his talk, I invited him to use O K-XAFS experiments in our center. Since then, he has been one of influential and powerful users and has worked on many subjects of new batteries [88-96]. He developed various kinds of innovative batteries, based on the elemental strategy. First and impressive work was about a newly developed battery ( $\text{Li}_{1.3}\text{Nb}_{0.3}\text{Mn}_{0.4}\text{O}_2$ ) with very high energy density. Charge/discharge profiles are shown in Fig. 66, indicating high-reversible capacities of 250–300 mAh/g at 50 °C, compared with the conventional  $\text{LiCoO}_2$  battery. In this study,  $\text{Nb}^{5+}$  ions were chosen to stabilize the redox reaction of oxide ions. Large reversible capacity originates from the solid-state redox of oxide ions coupled with transition metal redox, as shown in Fig. 67. Here, again, importance of oxygen in the redox reaction was stressed. It was revealed that many oxides containing  $\text{Li}^+$ , which had been originally thought to be electrochemically inactive, such as  $\text{Li}_3\text{NbO}_4$ , can potentially be



**Fig. 65.** Dr. Yabuuchi (Prof. of Yokohama National University) at the invited talk of the annual meeting of the SR center in 2017.

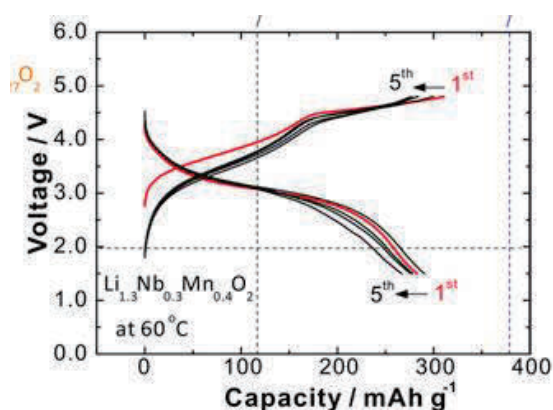


**Fig. 66.** Charge/discharge profiles at 60°C of  $\text{Li}_{1.3}\text{Nb}_{0.3}\text{Mn}_{0.4}\text{O}_2$ . Reprinted from Ref. 88 by courtesy of PNAS.

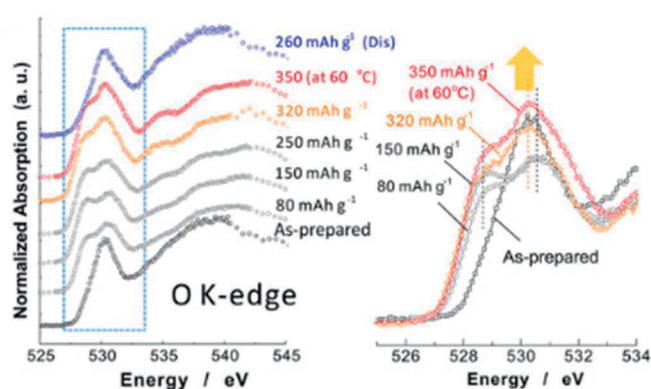


**Fig. 67.** O K-edge XAFS of  $\text{Li}_{1.3}\text{Nb}_{0.3}\text{Mn}_{0.4}\text{O}_2$  in the charge and discharge processes. The spectra in the pre-edge region (right) indicate the involvement of O in the redox reaction. Reprinted from Ref.88 by courtesy of PNAS.

used as the new host structures for high-capacity electrode materials. This work was published in PNAS [88], which was chosen as a top 1% cited paper. Again, Prof. Yabuuchi is one of the great contributors of the scientific activities of the center.

### (7) Visualization of the charge/discharge mechanism

As described in previous section, Prof. Inada's group has developed a wide area imaging XAFS technique for the spatial analysis of a different oxidation state of transition metal species. They applied this technique to trace how charge/discharge of the  $\text{LiFePO}_4$  electrode proceeds [54]. Figure 68 shows the changes of the Fe(III) and Fe(II) distributions during two successive charge/discharge cycles. The charge/discharge proceeds inhomogeneously and, interestingly, the electrode reaction starts at the same spots both in the charge and discharge processes, and the redox reactions of the Fe species occur reversibly.

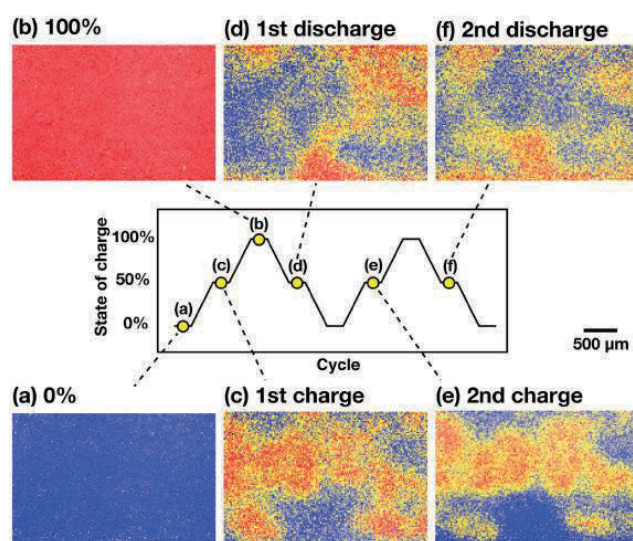


**Fig. 68.** Chemical state mapping obtained by the *in situ* XAFS imaging measurements during two successive charge/discharge cycles. 100% Fe(III) and 100 % Fe(II) are shown as red and blue colors, respectively. Reprinted from Ref. 54 with permission of Elsevier.

The maps of the 1<sup>st</sup> and 2<sup>nd</sup> charge/discharge are similar to each other, indicating high reproducibility and reversibility of the inhomogeneous electrode reaction. Note that such inhomogeneous reactions are specific to the LFP electrode. Other electrodes exhibit other type of reactions, which must be related to local ion and electron conduction. This is a typical example to demonstrate how complicated the battery reactions are.

Another example of application is to visualize the cross-sectional reaction distribution of the same  $\text{LiFePO}_4$  electrode, conducted by Dr. Oriksa in Prof. Uchimoto's laboratory of Kyoto University [97]. They prepared composite electrodes with different porosity by applying pressures of 300 kgf, 600 kgf, 900 kgf, and 1200 kgf.

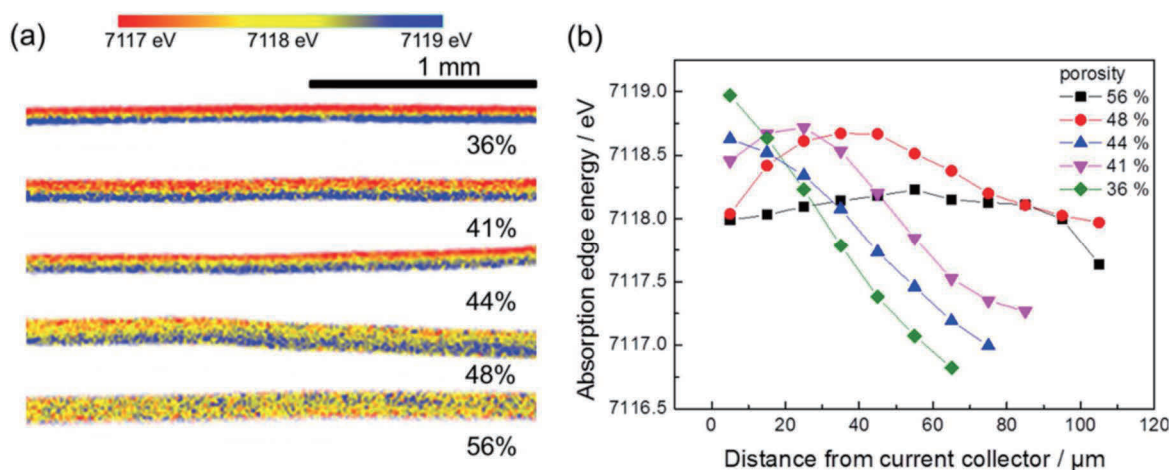


**Fig. 69.** (a) Cross section 2D mapping of absorption energy at Fe K-edge in LiFePO<sub>4</sub> composite electrodes. Current collector is located at the bottom side. (b) Absorption edge energy as a function of distance from the current collector for each sample with a different porosity. Reprinted from Ref. 97. Copyright (2016), Springer Nature.

By using a cross section polisher, Fe K-edge imaging XAFS was obtained for the cross section of each sample. Results are shown in Fig. 69, where the porosity was estimated from the applied pressure and SEM image.

In the figure, color change from blue to red indicates that the discharge reaction proceeds. Apparently inhomogeneous reaction is caused especially for low porosity electrodes. When the porosity of the electrode was 44 %, 41 %, 36 %, the reaction occurs preferentially from electrode / electrolyte interface. However, when the porosity of the electrode is 56 % or 48 %, the uniform reaction is achieved. For the design principle of composite electrodes, it is essential to understand the relationship among battery performance, reaction distribution and electronic/ionic conductivity in composite electrodes. These works demonstrate that the imaging XAFS would provide a guideline for practical production of batteries.

### (8) Soft X-ray microscopic study of cyanobacteria

Soft x-ray microscopy (SXM) is a minimally invasive technique for single-cell high-resolution imaging as well as the visualization of intracellular distributions of light elements such as carbon, nitrogen, and oxygen. The soft X-ray microscopy beamline (BL-12) has been operated since 1997 and presented demonstrative works with various images, but no scientifically impressive output. Recently, Drs. Teramoto and Azai of Ritsumeikan University applied SXM to the study of photosynthesis and nitrogen fixation in the filamentous cyanobacterium *Anabaena sp.* PCC 7120, in which vegetative cells are converted to heterocysts during nitrogen starvation. Structural model of the cyanobacteria is shown in Fig.70. Statistical and spectroscopic analyses of the SXM images

around the K-absorption edge of nitrogen revealed a significant difference in the carbon-to-nitrogen (C/N) ratio between vegetative cells and heterocysts. Application of this analysis to soft X-ray images of *Anabaena sp.* PCC 7120 revealed inhomogeneous C/N ratios in the cells. Furthermore, soft X-ray tomography of *Anabaena sp.* PCC 7120 enabled us to visualize 3D images of C and N inhomogeneous distributions of in vivo vegetative cells and heterocysts, as shown in Fig. 71. This work was published in *Physiology Plant* as one of breakthrough technology [98].

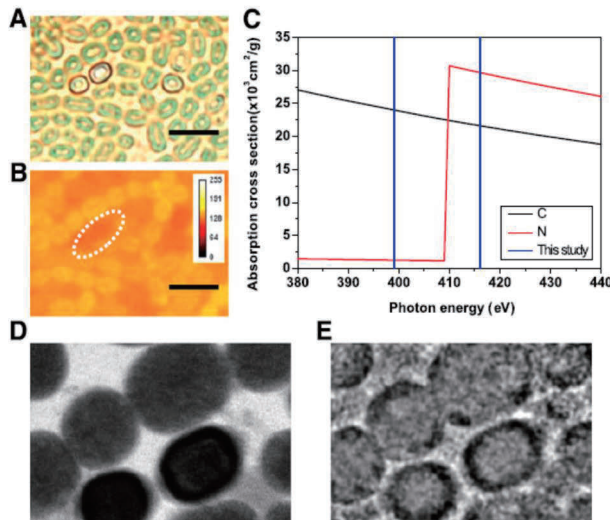


**Fig.70.** Soft x-ray images of *Anabaena sp.* PCC 7120. **A** and **B**, Heterocysts and vegetative cells in *Anabaena sp.* PCC 7120 observed using optical microscopy (**A**) and fluorescence microscopy (**B**). Heterocysts are identified in white circles. **C**, Photoabsorption cross section around the N1s absorption edge. **D** and **E**, Soft x-ray images of *Anabaena sp.* PCC 7120 observed at a photon energy of 398 eV (below the N1s edge) and 416 eV (above the N1s edge), respectively. Bars 10 mm (**A** and **B**) and 2 mm (**D** and **E**). Reprinted from Ref. 98. Copyright (2018), Oxford University Press.

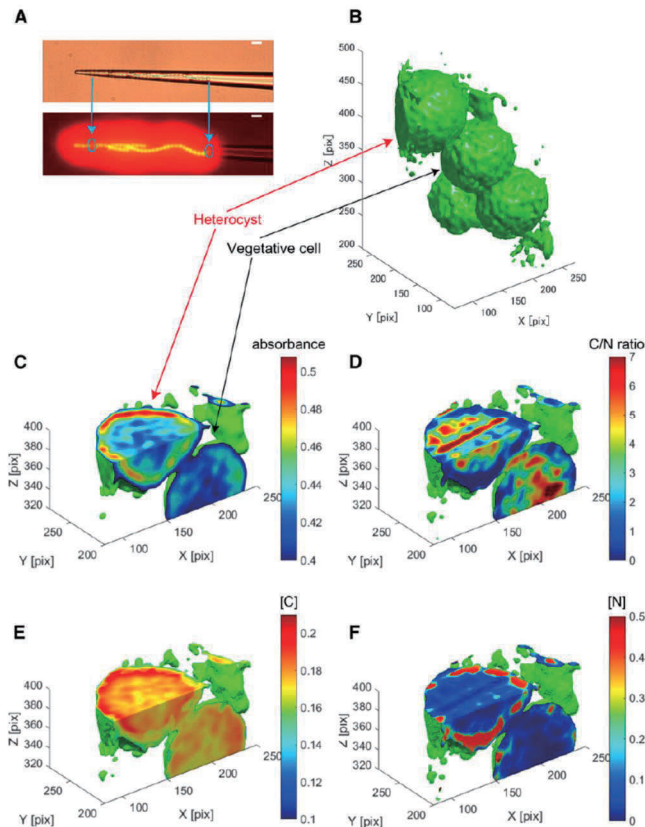


**Fig.71.** 3D distribution of C/N and C and N concentrations in the cells in *Anabaena sp.* PCC 7120. **A**, Optical and fluorescence images of *Anabaena sp.* PCC 7120 in the capillary. **B**, 3D display of a tomographic image of *Anabaena sp.* PCC 7120 measured at a photon energy of 398 eV. **C**, Cross-sectional display of the tomographic image of **B**. **D**, Cross sectional display of C/N tomography. **E** and **F**, Cross-sectional display of reductant C (**E**) and N (**F**) concentration distribution. Units in the color bar for **C** and **D** are arbitrary units, but correspond to  $\text{pg}/\mu\text{m}^3$  in **E** and **F**. Bars in **A** = 10 mm. Reprinted from Ref. 98. Copyright (2018), Oxford University Press.

## 2.7 Education, outreach activities and miscellaneous

Since the center is a subsidiary of Ritsumeikan University, one of the missions should be education of the advanced technology, synchrotron radiation for graduate and under graduate students. With the help of Prof. Namba, we asked Department of Physics to incorporate SR experiments in the curriculum of physics experiments in the third year. It started in fiscal 2008 in the first half semester for 6 times every Wednesday afternoon, consisting of a lecture of synchrotron radiation by the director on the first day, following with several specific experiments, such as soft X-ray spectroscopy, soft X-ray microscopy, Photoelectron spectroscopy for four days under the guide by the staffs, and the presentation of each experiment on the last day. This was a unique curriculum, performable only in a university having an SR center. It continued until 2014 and unfortunately ended because of lack of manpower.

In the Department of Applied Chemistry of Faculty of Life Sciences, Profs. Inada and Ozutsumi have incorporated the XAFS experiments at BL-3 and 4 in the curriculum of experiments in the third year.

As one of outreach activities, we have held once a year the on-site visit, lecture and one day training of synchrotron radiation for 20 ~ 30 applicants in Ritsumeikan-affiliated high schools. After the lecture, they are divided into 4 or 5 groups for specific experiments. Next day after the training of several specific experiments, they present about the experiments involved. This training course is also unique and favorable for high school pupils. Several times, pupils from KSA (Korean Science Academy) joined this program. In such case, communication and presentations were all



**Fig. 72.** A scene of practical training of high school pupils at the X-ray microscopy beamline (BL-12) on July 30, 2008.

in English, which might be useful for future. Photo in Fig. 72 shows a scene of the experimental training. It continued from 2006 to 2019, but interrupted by COVID19. I hope it will restart after corona.

Last but not least is that the SR center served as a host for the annual meeting of JSSR (Japanese Society of Synchrotron Radiation) in 2008. It has become a custom that every facility hosts the annual meeting by turns. However, SR center had refused to be the host so far because of lack of manpower. In fact, different from other facilities, there were not so many members of JSSR in Ritsumeikan. However, I found it necessary to accept the host in order to make the SR center



**Fig. 73.** (Left) A scene of company's exhibition at a corridor of Co-Learning I building in the Biwako-Kusatsu Campus, Ritsumeikan University. (Right) Banquet held at the Biwako hotel in Otsu.

recognized as one of the SR facilities in Japan. It was a challenge to accept with a limited staff in the center and few members in faculties, but with great help of CREOTEC and intensive users nearby, the meeting was held successfully. Ritsumeikan has many classrooms to accommodate huge numbers of participants, but poster presentations and company's exhibitions should be held at a long and wide corridor which has no heating hardware. It was a serious problem how to protect participants from severe coldness in January. We had to seal off every exit with vinyl sheets and deliver handy warmers to participants. Figure 73 shows photos of the annual meeting of JSSR in 2008. We accepted the host again in 2015 and the meeting was held without serious troubles, since we had knowhow of the meeting and the member of JSSR increased in our university. And the next annual meeting of JSSR will be held in Ritsumeikan under the serious situation of CORONA.

### 3. Future prospect

In Fiscal 2019, the director of SR center was taken over to Prof. Kazuo Kojima, with support by Prof. Inada as the sub-director. Soon after the new system started in 2021, a serious trouble of the ring happened unfortunately. It was worried to be a fatal damage, but the ring was completely recovered and restarted operation in April, 2022.

The situation of Japanese synchrotron radiation has dramatically changed since 2006. In 2011, Aichi synchrotron radiation research center started the operation and in 2019, the Slit-J project was approved and a high brilliant 3 GeV ring is now under construction at Aoba-yama campus of Tohoku University, expecting the commissioning in 2024, as a new facility named, "Nano-Terasu". Someone says that there exist too many SR facilities in Japan. In fact, 70 % of SR facilities in the world are concentrated in a small country, Japan. However, judging whether there are too many or not should depend on how much actively they are used. When Aichi started operation, it was

believed that most of the users in Ritsumeikan would move to Aichi, but there are still many users in the center. Certainly, number of synchrotron users increases year by year. It is a unique feature of Japan that everyone can access synchrotron facilities without high barrier.

Recently, the grade of Japan is rapidly going down in the world both in economy and science. How to compete with foreign countries and survive in the world is an urgent matter. Only way, I believe, is to accelerate the development of science and technology, and to develop new functional materials one after another. For that purpose, advanced tools are necessary to characterize such materials. Synchrotron radiation is one of the advanced techniques, now familiar to researchers, different from other countries. It must be a big advantage for Japan to have many SR facilities!

However, to meet the needs from users, every kind of improvement is necessary in synchrotron radiation science. AURORA is the oldest accelerator actively used in Japan and possibly in the world. We must improve the performance, and also plan to renew the accelerator sooner or later.

There are several constraints if it will be constructed in the University campus. One is the size of accelerators, which should be compact enough to be installed in the existing center building. Second is the performance, which should be better than the present one. The present machine is completely circular and the gap of the superconducting magnet is as wide as 250 mm to incorporate an RF cavity in the circle of the electron orbit, as shown in Fig.1. If the RF cavity could be taken away from the magnet, the magnet gap can be much narrower and as a result of it, we could obtain synchrotron radiation with higher intensity and higher energy than the present one, as shown in Fig. 74[99]. This might be realized by constructing a race track type storage ring like ASURORA-2 and HiSOR ring. However, different from them, superconducting magnet is essential, whose recent improvement is remarkable. With this new type of storage ring, available X-ray energy will extend up to 20 keV and more users will be expected. The last, but most important is the budget. In fact, it is too much for one private university to construct and maintain such an expensive instrument. For future, we had better organize a new system for the new SR project, such as a consortium composed of the local government, universities and companies nearby. It is not an easy task, but worth challenging. Finally, I would like to close my review, praying further development and prosperity of the SR center hereafter.

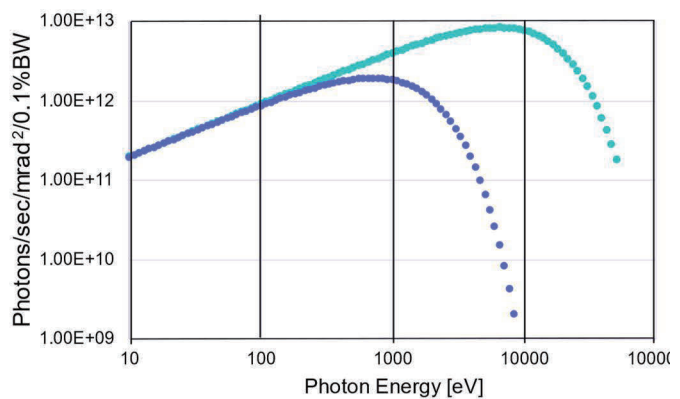


**Fig. 74.** Photon energy distributions of synchrotron radiation from the present machine ( $E=0.575$  GeV,  $B=3.73$  T) blue plots, and from the planning machine ( $E=1.2$  GV,  $B=8$ T), green plots. [99]

## References

- [1] N. Takahashi, *Nucl. Instrum. Methods Phys. Res. B*, **1987**, 24-25, 425.
- [2] T. Takayama, *Nucl. Instrum. Methods Phys. Res. B*, **1987**, 24-25, 420.
- [3] H. Iwasaki, Y. Nakayama, K. Ozutsumi, Y. Yamamoto, Y. Tokunaga, H. Saisho and T. Matsubara, *J. Synchrotron Radiation*, **1998**, 5, 1162.
- [4] E.W. Becker, W. Ehrfeld, et al, *Naturwissenschaften*, **1982**, 69, 520.
- [5] E.W. Becker, W. Ehrfeld, et al, *Microelectronic Engineering*, **1986**, 4, 35.
- [6] Y. Kido, H. Namba, T. Nishimura, A. Ikeda, Y. Yan and A. Yagishita, *Nucl. Instrum. Methods Phys. Res. B*, **1998**, 136-138, 798.
- [7] T. Nishimura, Y. Hoshino, H. Namba and Y. Kido, *Sur. Sci.*, **2000**, 461, 146.
- [8] H. W. Yeom, H. Hamamatsu, T. Ohta and R. I. G. Uhrberg, *Phys. Rev. B*, **1999**, 59, R10413.
- [9] G. Schmal, D. Rudolph, B. Niemann, P. Gutmann, J. Thieme, G. Schneider, C. David, M. Diehl, and T. Wilhein, *Optik*, **1993**, 93, 95.
- [10] A. Hirai, K. Takemoto, K. Nishino, B. Niemann, M. Hettwer, D. Rudolph, E. Anderson, E. Anderson, D. Attwood, D. P. Kern, Y. Nakayama, and H. Kihara, *Jpn. J. Appl. Phys.*, **1999**, 38, 274.
- [11] H. Daimon, *Rev. Sci. Instrum.*, **2001**, 72, 2633.
- [12] S. Sugiyama, Y. Zhang, H. Ueno, M. Hosaka, T. Fujimoto, R. Maeda, and T. Tanaka, *MHS'96 (7<sup>th</sup> International Symposium on Micromachine and Human Science)*, **1996**, 96, 79.
- [13] O. Tabata, K. Terasoma, N. Agawa, and K. Yamamoto, *12<sup>th</sup> IEEE Int. Conf. on Micro Electro Mechanical Systems*, **1999**, 99, 252.
- [14] O. Tabata, K. Terasoma, N. Agawa, and K. Yamamoto, *IEEJ Transactions on Sensors and Micromachines*, **2000**, 120, 321.
- [15] S. Sugiyama, S. Khumpuang and G. Kawaguchi, *J. Microcech. Micreng.*, **2004**, 14, 1399.
- [16] Y. Zhang and T. Katoh, *Jpn. J. Appl. Phys.*, **1996**, 35, 186.
- [17] N. Nishi, T. Katoh, H. Ueno, S. Konishi, and S. Sugiyama, *Proc. MHS'99*, **1999**, 93.
- [18] T. Nishimura, A. Ikeda, H. Namba, T. Morishita, and Y. Kido, *Surf. Sci.*, **1999**, 421, 273.
- [19] Y. Kido, T. Nishimura, Y. Hoshino, and H. Namba, *Nucl. Instrum. Methods B*, **2000**, 161-163, 371.
- [20] T. Nishimura, Y. Hoshino, H. Namba and Y. Kido, *Nucl. Instrum. Methods A*, **2001**, 467-468, 1237.
- [21] Y. Hoshino, T. Nishimura, T. Yoneda, K. Okawa, H. Namba and Y. Kido, *Surf. Sci.*, **2002**, 505, 234.
- [22] Y. Hoshino, T. Nishimura, Y. Taki, Y. Asami, K. Sumitomo and Y. Kido, *Surf. Sci.*, **2002**, 511, 112.
- [23] Y. Hoshino, Y. Kido, K. Yamamoto, S. Hayashi and M. Niwa, *Appl. Phys. Lett.*, **2002**, 81, 2650.

- [24] Y.Hoshino, S.Matsumoto, and Y.Kido, *Surf. Sci.*, **2003**, 531, 295.
- [25] Y. Hoshino, S. Matsumoto, K. Ogawa, H. Namba and Y. Kido, *Phys. Rev. B*, **2003**, 68, 073308.
- [26] Y. Hoshino, O. Kitamura, T. Nakada and Y. Kido, *Surf. Sci.*, **2003**, 539, 14.
- [27] Y. Hoshino, S. Matsumoto, T. Nakada and Y. Kido, *Surf. Sci.*, **2004**, 556, 78.
- [28] Y. Hoshino, R. Fukuyama and Y. Kido, *Phys. Rev. B*, **2004**, 70, 165303.
- [29] T. Nishimura, T. Okazawa, Y. Hoshino, Y. Kido, K. Iwano, K. Tominaga, T. Nabatame, and A. Toriumi, *J. Appl. Phys.*, **2004**, 96, 6113.
- [30] T. Nishimura, J. Takeda, A. Asami, Y. Hoshino, and Y. Kido, *Surf. Sci.*, **2005**, 588, 71.
- [31] Y. Hoshino, Y. Matsubara, T. Nishimura and Y. Kido, *Phys. Rev. B*, **2005**, 72, 235416.
- [32] F. Matsui, Y. Hori, H. Miyata, N. Sugiyama, H. Daimon, *Appl. Phys. Lett.*, **2002**, 81, 2556.
- [33] H. Namba, K. Yamamoto, T. Ohta, and H. Kuroda, *J. Electron Spectrosc. Relat. Phenom.*, **1998**, 88-91, 707.
- [34] K. Ogawa, N. Fujisawa, K. Nakanishi and H. Namba, *e-J. Surf. Sci. Nanotech.*, **2006**, 4, 494.
- [35] J. Tsuji, K. Kojima, S. Ikeda, H. Nakamatsu, T. Mukoyama, and K. Taniguchi, *J. Synchro. Rad.*, **2001**, 8, 554.
- [36] J. Tsuji, K. Kojima, S. Ikeda, H. Nakamatsu, T. Mukoyama, and K. Taniguchi, *X-ray Spectrometry*, **2002**, 31, 319.
- [37] H. Oji, T. Tominaga, K. Nakanishi, M. Ohmoto, K. Ogawa, M. Kimura, S. Kimura, T. Okamoto and H. Namba, *J. Electron Spectrosc. Relat. Phenom.*, **2006**, 152, 121.
- [38] T. Ohta and Y. Yamamoto, *Patent No. 2006-198923* “Electron Storage Ring”.
- [39] T. Yaji, Y. Yamamoto, T. Ohta and S. Kimura, *Infrared Phys. Tech.*, **2008**, 51, 397.
- [40] T. Kawasaki, T. Yaji, T. Imai, T. Ohta, K. Tsukiyama, *Am. J. Anal. Chem.*, **2014**, 5, 384.
- [41] T. Kawasaki, T. Yaji, T. Ohta and K. Tsukiyama, *J. Synchrotron Rad.*, **2016**, 23, 152.
- [42] T. Kawasaki, T. Yaji, T. Ohta, K. Tsukiyama, K. Nakamura, *Cell. Mol. Neurobio.*, **2018**, 38, 1039.
- [43] T. Kawasaki, T. Sakai, H. Zen, Y. Sumitomo, K. Nogami, K. Hayakawa, Ken, T. Yaji, T. Ohta, T. Tsukiyama, Y. Hayakawa, *ACS Energy & Fuels*, **2020**, 34, 9064.
- [44] T. Kawasaki, Y. Yamaguchi, T. Ueda, Y. Ishikawa, T. Yaji, T. Ohta, K. Tsukiyama, T. Idehara, M. Saiki, and M. Tani, *Biomedical Optics Express*, **2020**, 11, 5341.
- [45] Y. Kittaka, T. Hayashi, A. Honda, M. Yoshimura, S. Kuretake, N. Tanaka, A. Ando and H. Takagi, *J. Am. Ceram. Soc.*, **2012**, 95, 2899.
- [46] M. Ogawa, T. Yaji, K. Nakanishi, and T. Ohta, *Adv. X-ray Chem. Anal. Japan*, **2016**, 47, 311.
- [47] K. Nakanishi, D. Kato, H. Arai, H. Tanida, T. Mori, Y. Orikasa, Y. Uchimoto, T. Ohta and Z. Ogumi, *Rev. Sci. Instrum.*, **2014**, 85, 084103.
- [48] K. Yamanaka, K. Nakanshi, I. Watanabe, and T. Ohta, *Electrochem.*, **2018**, 86, 128.
- [49] T. Yaji, T. Ohta and K. Amemiya, *Memoirs of The SR center, Ritsumeikan Univ.*, **2013**, 15, 153.

- [50] K. Mitsuhashi, T. Yaji and T. Ohta, *Memoirs of The SR center, Ritsumeikan Univ.*, **2014**, *16*, 159.
- [51] M. Katayama, K. Sumiwaka, M. Sato, K. Ozutsumi, and Y. Inada, *Memoirs of The SR center, Ritsumeikan Univ.*, **2011**, *13*, 15.
- [52] M. Katayama, K. Sumiwaka, K. Hayashi, K. Ozutsumi, T. Ohta and Y. Inada, *J. Synchro. Rad.*, **2012**, *19*, 717.
- [53] K. Sumiwaka, M. Katayama and Y. Inada, *Memoirs of The SR center, Ritsumeikan Univ.*, **2012**, *14*, 11.
- [54] M. Katayama, K. Sumiwaka, R. Miyahara, H. Yamashige, H. Arai, Y. Uchimoto, T. Ohta, Y. Inada, and Z. Ogumi, *J. Power Sources*, **2014**, *269*, 994.
- [55] M. Katayama, R. Miyahara, T. Watanabe, H. Yamagishi, S. Yamashita, T. Kizaki, T. Sugawara, and Y. Inada, *J. Synchrotron Rad.*, **2015**, *22*, 1227.
- [56] M. Katayama, H. Yamagishi, Y. Yamamoto and Y. Inada, *Anal. Sci.*, **2020**, *36*, 47.
- [57] H. Okamoto, Y. Kumai, Y. Sugiyama, T. Mitsuoka, K. Nakanishi, T. Ohta, N. Satoshi, S. Shirai, and H. Nakano, *J. Am. Chem. Soc.*, **2010**, *132*, 2710.
- [58] Y. Sugiyama, H. Okamoto, T. Mitsuoka, T. Morikawa, K. Nakanishi, T. Ohta, and H. Nakano, *J. Am. Chem. Soc.*, **2010**, *132*, 5946.
- [59] H. Nakano, M. Nakano, K. Nakanishi, D. Tanaka, Y. Sugiyama, T. Ikuno, H. Okamoto, and T. Ohta, *J. Am. Chem. Soc.*, **2012**, *134*, 5452.
- [60] M. Ohashi, H. Nakano, T. Morishita, M. J. S. Spencer, Y. Ikemoto, C. Yogi and T. Ohta, *Chem. Commun.*, **2014**, *50*, 9761.
- [61] H. Okamoto, Y. Sugiyama, K. Nakanishi, T. Ohta, T. Mitsuoka, and H. Nakano, *Chem. Mater.*, **2015**, *27*, 1292.
- [62] H. Maruyama, H. Nakano, M. Ogawa, M. Nakamoto, T. Ohta, and A. Sekiguchi, *Sci. Rep.*, **2015**, *5*, 13219.
- [63] Y. Imada, H. Nakano, K. Furukawa, R. Kishi, M. Nakano, H. Maruyama, M. Nakamoto, A. Sekiguchi, M. Ogawa, T. Ohta, and Y. Yamamoto, *J. Am. Chem. Soc.*, **2016**, *138*, 479.
- [64] H. Senoh, T. Takeuchi, H. Kageyama, H. Sakaebe, M. Yao, K. Nakanishi, T. Ohta, T. Sakai, and K. Yasuda, *J. Power Sources*, **2010**, *195*, 8327.
- [65] T. Takeuchi, H. Kageyama, K. Nakanishi, M. Tabuchi, H. Sakaebe, T. Ohta, H. Senoh, T. Sakai, and K. Tatsumi, *J. Electrochem. Soc.*, **2010**, *157*, A1196.
- [66] H. Senoh, H. Kageyama, T. Takeuchi, K. Nakanishi, T. Ohta, H. Sakaebe, M. Yao, T. Sakai, K. Yasuda, *J. Power Sources*, **2011**, *196*, 5631.
- [67] T. Takeuchi, H. Kageyama, K. Nakanishi, Y. Inada, M. Katayama, T. Ohta, H. Senoh, H. Sakaebe, T. Sakai, K. Tatsumi, and H. Kobayashi, *J. Electrochem. Soc.*, **2012**, *159*, A75.
- [68] T. Takeuchi, H. Kageyama, K. Nakanishi, T. Ohta, A. Sakuda, H. Sakaebe, H. Kobayashi, K. Tatsumi, and Z. Ogum, *ECS Electrochem. Lett.*, **2014**, *3*, A31.

- [69] T. Takeuchi, H. Kageyama, K. Nakanishi, T. Ohta, A. Sakuda, T. Sakai, H. Kobayashi, H. Sakaebe, K. Tatsumi, and Z. Ogumi, *Solid State Ionics*, **2014**, *262*, 138.
- [70] T. Takeuchi, H. Kageyama, K. Nakanishi, M. Ogawa, T. Ohta, A. Sakuda, H. Sakaebe, H. Kobayashi, and Z. Ogumi, *J. Electrochem. Soc.*, **2015**, *162*, A1745.
- [71] T. Takeuchi, H. Kageyama, M. Ogawa, K. Mitsuhara, K. Nakanishi, T. Ohta, A. Sakuda, H. Kobayashi, H. Sakaebe, Z. Ogumi, *Solid State Ionics*, **2016**, *288*, 199.
- [72] E. Yilmaz, C. Yogi, K. Yamanaka, T. Ohta, and H. R. Byon, *Nano Letters.*, **2013**, *13*, 4679.
- [73] N. Bonnet-Mercier, R. A. Wong, M. L. Thomas, A. Dutta, K. Yamanaka, C. Yogi, T. Ohta and H. R. Byon, *Sci. Rep.*, **2014**, *4*, 7127.
- [74] M. L. Thomas, K. Yamanaka, T. Ohta and H. R. Byon, *Chem. Comm.*, **2015**, *51*, 3977.
- [75] C. Yang, R. Wong, K. Yamanaka, T. Ohta, H. R. Byon, *Nano Letters*, **2016**, *16*, 2969.
- [76] R. A. Wong, A. Dutta, C. Yanga, K. Yamanaka, T. Ohta, S.-H. Yoone, A. Nakao, K. Waki and H. R. Byon, *Chem. Mater.*, **2016**, *28*, 8006.
- [77] A. Dutta, R.A. Wong, W. Park, K. Yamanaka, T. Ohta, Y. Jung, and H. R. Byon, *Nature Commun.*, **2018**, *9*, 680.
- [78] R. A. Wong, C. Yang, A. Dutta, M. O, M. Hong, M. L. Thomas, K. Yamanaka, T. Ohta, K. Waki, and H. R. Byon, *ACS Energy Letters*, **2018**, *3*, 592.
- [79] H. Oh, H. Yamagishi, T. Ohta and H. R. Byon, *Materials Chemistry Frontiers*, **2021**, *5*, 3657.
- [80] C. Yogi, D. Takamatsu, K. Yamanaka, H. Arai, Y. Uchimoto, K. Kojima, I. Watanabe, T. Ohta, Z. Ogumi, *J. Power Sources*, **2014**, *248*, 994.
- [81] A. Yano, M. Shikano, H. Kanzaki, K. Yamanaka, H. Kageyama, and T. Ohta, *J. Electrochem. Soc.*, **2017**, *164*, A3848.
- [82] Z. Lu and J.R. Dahn, *J. Electrochem. Soc.*, **2002**, *149*, A815.
- [83] M. Oishi, C. Yogi, I. Watanabe, T. Ohta, Y. Orikasa, Y. Uchimoto, and Z. Ogumi, *J. Power Sources*, **2015**, *276*, 89.
- [84] M. Oishi, K. Yamanaka, I. Watanabe, K. Shimoda, T. Matsunaga, H. Arai, Y. Ukyo, Y. Uchimoto, Z. Ogumi and T. Ohta, *J. Mater. Chem. A*, **2016**, *4*, 9293.
- [85] K. Shimoda, M. Oishi, T. Matsunaga, M. Murakami, K. Yamanaka, H. Arai, Y. Ukyo, Y. Uchimoto, T. Ohta, E. Matsubara, Z. Ogumi, *J. Mater. Chem. A*, **2017**, *5*, 6695.
- [86] M. Sathiy, G. Rouse, K. Ramesha, C. P. Laisa, H. Vezin, M. T. Sougrati, M. L. Doublet, D. Foix, D. Gonbeau, W. Walker, A. S. Prakash, M. B. Hassine, L. Dupont, and J.-M. Tarascon, *Nature Materials*, **2013**, *12*, 827.
- [87] N. Yabuuchi, K. Yoshii, S-T. Myung, I. Nakai, and S. Komaba, *J. Am. Chem. Soc.*, **2011**, *133*, 4404.
- [88] N. Yabuuchi, M. Takeuchi, M. Nakayama, H. Shiiba, M. Ogawa, K. Nakayama, T. Ohta, D. Endo, T. Ozaki, T. Inamasu, and S. Komaba, *Proc. Natl Acad. Sci. U. S. A.*, **2015**, *112*, 7650.
- [89] T. Matsuhara, Y. Tsuchiya, K. Yamanaka, K. Mitsuhara, T. Ohta, N. Yabuuchi,

*Electrochemistry*, **2016**, *84*, 797.

[90] Y. Tsuchiya, K. Takanashi, T. Nishinobo, A. Hokura, M. Yonemura, T. Matsukawa, T. Ishigaki, K. Yamanaka, T. Ohta, and N. Yabuuchi, *Chem. Mater.*, **2016**, *28*, 7006.

[91] K. Sato, M. Nakayama, A. Glushenkov, T. Mukai, Y. Hashimoto, K. Yamanaka, M. Yoshimura, T. Ohta, N. Yabuuchi, *Chem. Mater.*, **2017**, *29*, 5043.

[92] N. Yabuuchi, M. Nakayama, M. Takeuchi, S. Komaba, Y. Hashimoto, T. Mukai, H. Shiiba, K. Sato, Y. Kobayashi, A. Nakao, M. Yonemura, K. Yamanaka, K. Mitsuhashi, T. Ohta, *Nature Communications*, **2016**, *7*, 13814.

[93] T. Kobayashi, W. Zhao, H. B. Rajendra, K. Yamanaka, T. Ohta, and N. Yabuuchi, *Small*, **2019**, *16*, 1902462.

[94] K. Yamamoto, Y. Zhou, N. Yabuuchi, K. Nakanishi, T. Yoshinari, T. Kobayashi, Y. Kobayashi, R. Yamamoto, A. Watanabe, Y. Orikasa, K. Tsuruta, J. Park, H. R. Byon, Y. Tamenori, T. Ohta and Y. Uchimoto, *Chem. Mater.*, **2020**, *32*, 139.

[95] Y. Kobayashi, M. Sawamura, S. Kondo, M. Harada, Y. Noda, M. Nakayama, S. Kobayakawa, W. Zhao, A. Nakao, A. Yasui, H. B. Rajendra, K. Yamanaka, T. Ohta, and N. Yabuuchi, *Materials Today*, **2020**, *37*, 43.

[96] R. Fukuma, M. Harada, W. Zhao, M. Sawamura, Y. Noda, M. Nakayama, M. Goto, D. Kan, Y. Shimakawa, M. Yonemura, N. Ikeda, R. Watanuki, H. L. Andersen, A. M. Angelo, N. Sharma, J. Park, H. R. Byon, S. Fukuyama, Z. Han, H. Fukumitsu, M. S. Dobrick, K. Yamanaka, H. Yamagishi, T. Ohta, and N. Yabuuchi, *ACS Cent. Sci.*, **2022**, *8*, 775.

[97] Y. Orikasa, Y. Gogyo, H. Yamashige, M. Katayama, K. Chen, T. Mori, K. Yamamoto, T. Masese, Y. Inada, T. Ohta, Z. Siroma, S. Kato, H. Kinoshita, A. H. Arai, Z. Ogumi, and Y. Uchimoto, *Sci. Rep.*, **2016**, *6*, 26382.

[98] T. Teramoto, C. Azai, K. Terauchi, M. Yoshimura, and T. Ohta, *Plant Physiology*, **2018**, *177*, 52.

[99] Y. Yamamoto, *private communication*.